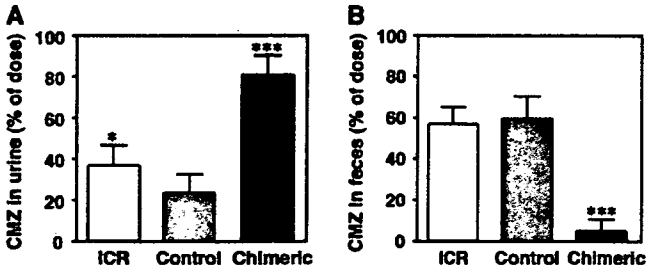

FIG. 1. CMZ excretion in chimeric mice with humanized liver. CMZ in urine (A) and in feces (B) was determined as described in "Materials and Methods" section. Data represent the mean ± SD. ICR, ICR mice (n = 6); control, uPA$^{-/-}$/SCID mice (n = 7); and chimeric, chimeric mice (n = 5). $*p < 0.05$, $***p < 0.001$, compared with control.

Expression of Human Drug Transporter in Chimeric Mice

The hepatic mRNA expression of human transporters in the chimeric mice is shown in Table 4. P-gp, BSEP, MRP2, and BCRP can transport a substrate into the bile duct from hepatocytes. OCT1, OATP1B1, and OATP1B3 can uptake a substrate into hepatocytes. Human transporters were expressed in the liver of all chimeric mice used in this study (Table 4). Because the anti-human transporter antibodies commercially available cross-react with mouse orthologous transporters, the protein expression level could not be measured.

Expression of Mouse Drug Transporter in Chimeric Mice

The hepatic mRNA expression of mouse transporters in the chimeric mice is shown in Table 5. The hepatic mRNA expression of mouse mdr1, bsep, mrp2, and bcrp in chimeric mice was 190, 31, 19, and 20% of that in control uPA$^{-/-}$/SCID mice, respectively. The mRNA expression of mouse oct1 and oatp1b2 in chimeric mice was 4 and 4% of that in uPA$^{-/-}$/SCID mice, respectively.

Drug-Stimulated Transporter ATPase Activity Assay

The affinity of CMZ to human P-gp and MRP2 was estimated by ATPase activity assay. No stimulation of vanadate-sensitive P-gp or MRP2 ATPase activity was observed up to 2 mM CMZ. Although human BCRP and BSEP membranes could not be obtained, CMZ did not stimulate the ATPase activity in rat Bcrp and Bsep membranes up to 1 mM CMZ.

DISCUSSION

Understanding the pharmacokinetics could support the efficient and safe evaluation of drug candidates during drug development. However, extrapolation from experimental animals to humans is difficult due to the species differences in absorption, distribution, metabolism, and excretion. There have been many reports that the cumulative excretion of radioactivity in urine and feces was different between species after administration of a ^{14}C-labeled drug (Karim *et al.*, 1976; Kolis *et al.*, 1976). In the present study, we focused on the species differences in excretion. In the case of CMZ, an unchanged form is mainly excreted. In humans, the cumulated CMZ excretion in urine was 79.7 ± 13.4% of the dose for 72 h after iv administration (Welage *et al.*, 1990) and was 68.8–86.0% of the dose for 24 h after im administration (Ko *et al.*, 1989). On the other hand, CMZ was mainly excreted into bile in rats (Murakawa *et al.*, 1980). In the preliminary study, the major excretory pathway was biliary excretion in ICR mice. Taking this information into consideration, CMZ was selected to investigate the humanization of the excretion pathway in chimeric mice. In humans, CMZ is usually administered iv. In mice, the CMZ excretion showed no significant difference between iv and ip administration. Therefore, excretion after an ip administration of CMZ was measured in the present study. In control uPA$^{-/-}$/SCID mice, biliary excretion of CMZ was the major pathway, reflecting the species differences in CMZ excretion between humans and mice. In chimeric mice, CMZ was mainly excreted in urine (Fig. 1). The present results suggested that the excretory profile of CMZ was humanized in the chimeric mice. The replacement with human hepatocytes of mouse liver seemed to affect the excretory profile of the drugs.

Recently, many drug transporters have been clarified to play important roles in drug excretion. In the present study, the expression of human and mouse drug transporters was investigated in the chimeric mice. In biliary excretion, the roles of human MDR1, BSEP, MRP2, and BCRP have been well characterized and were shown to be expressed on the canalicular membrane of hepatocytes. Human OCT1, OATP1B1, and OATP1B3 on the sinusoidal membrane, which may be involved in the uptake of a drug into hepatocytes, were also investigated. Human drug transporters were expressed in the liver of the chimeric mice, which was consistent with the previous report by Nishimura *et al.* (2005). For some human transporters, the relative mRNA expression in the chimeric mice was higher or lower than that in the donor hepatocytes. The mechanism of this phenomenon was unclear. Further study is needed to clarify the expression of human transporters in the chimeric mice generated using hepatocytes from various donors. In addition, the expressions of mouse drug transporters in chimeric mice were measured. Mouse oatp1b2 may correspond to human OATP1B1 (Hagenbuch and Meier, 2004). The expressions of mouse bsep, mrp2, bcrp, oct1, and oatp1b2 mRNAs in chimeric mice were lower than those in control uPA$^{-/-}$/SCID mice. The mRNA expression of some mouse cytochrome P450 enzymes in chimeric mice was described by Nishimura *et al.* (2005). The expression ratios of Cyp1a2, Cyp2c9, Cyp2e1, and Cyp3a11 mRNA, of which the mouse mRNA in chimeric mice to that in uPA$^{-/-}$/SCID mice, were 0.19 or less (Nishimura *et al.*, 2005). Their result was similar to those in our analysis. In the present study, the relative expressions in four out of six mRNAs were 0.20 or less (Table 5). It is presumed that 20% or less of mouse mRNA may be expressed in chimeric mice compared with

control uPA$^{-/-}$/SCID mice. The livers of the chimeric mice used in the present study were replaced approximately 80% by human hepatocytes; therefore, the residue of mouse mRNA was thought to be reasonable. Further study is needed to clarify whether the mouse protein retains its activity. Both the reduction of mouse transporter and the increase of human transporter expressions would be related to the humanization of excretory pattern in the chimeric mice.

The mRNA expression of human BCRP in chimeric mice was higher than that in donor hepatocyte. The mRNA expression of mouse mdr1 in chimeric mice was higher than that in control uPA$^{-/-}$/SCID mice. These results may be caused by the procedure of the generation of the chimeric mice or the knocking of the uPA gene, but the mechanism is unclear. It was clarified that CMZ was not a human P-gp and rat Bcrp substrate by the measurement of the ATPase activity using human P-gp and rat Bcrp. Therefore, the changes of the CMZ excretory profile in chimeric mice may be independent of the mouse mdr1 and human BCRP mRNA. The drug transporter for CMZ has not been identified yet. However, it should be possible that humanized drug transporters may influence the excretion in the chimeric mice. Although the present study did not investigate the humanization of other factors such as the physiology of liver and bile flow, we keep it in mind to discuss the mechanism.

There are a few reports on the species differences of the expression and substrate specificity in drug transporters. BCRP mRNA could be expressed in both liver and kidney in mice (Jonker *et al.*, 2000; Shimano *et al.*, 2003), but in liver and not in kidney in humans (Doyle *et al.*, 1998). Some compounds exhibited differences in the transport ratio between human and mouse P-gps (Yamazaki *et al.*, 2001). Taking the species differences of drug transporters into consideration, the chimeric mice could make some contribution to the understanding of drug transport involved in the excretion.

In conclusion, the excretory pattern of CMZ could be humanized in chimeric mice, suggesting that the chimeric mice can be useful in studies on drug excretion as well as drug metabolism. Further study concerning drug transporters is needed, but the present study would provide valuable information for applying pharmacological studies using chimeric mice with humanized liver.

ACKNOWLEDGMENTS

This work was supported by a Research on Advanced Medical Technology, Health, and Labor Sciences Research Grant from the ministry of Health, Labor, and Welfare of Japan. We acknowledge Mr Brent Bell for reviewing the manuscript.

REFERENCES

Angelin, B., Arvidsson, A., Dahlqvist, R., Hedman, A., and Schenck-Gustafsson, K. (1987). Quinidine reduces biliary clearance of digoxin in man. *Eur. J. Clin. Invest.* **17,** 262–265.

Chandra, P., and Brouwer, K. L. (2004). The complexities of hepatic drug transport: Current knowledge and emerging concepts. *Pharm. Res.* **21,** 719–735.

Doyle, L. A., Yang, W., Abruzzo, L. V., Krogmann, T., Gao, Y., Rishi, A. K., and Ross, D. D. (1998). A multidrug resistance transporter from human MCF-7 breast cancer cells. *Proc. Natl. Acad. Sci. U.S.A.* **95,** 15665–15670.

Faber, K. N., Muller, M., and Jansen, P. L. (2003). Drug transport proteins in the liver. *Adv. Drug Deliv. Rev.* **55,** 107–124.

Hagenbuc, B., and Meier, P. J. (2004). Organic anion transporting polypeptides of the OATP/SLC21 family: Phylogenetic classification as OATP/SLCO superfamily, new nomenclature and molecular/functional properties. *Pflugers Arch.* **447,** 653–665.

Hirom, P. C., Millburn, P., Smith, R. L., and Williams, R. T. (1972). Species variations in the threshold molecular-weight factor for the biliary excretion of organic anions. *Biochem. J.* **129,** 1071–1077.

Horikawa, M., Kato, Y., Tyson, C. A., and Sugiyama, Y. (2002). The potential for an interaction between MRP2 (ABCC2) and various therapeutic agents: Probenecid as a candidate inhibitor of the biliary excretion of irinotecan metabolites. *Drug Metab. Pharmacokinet.* **17,** 23–33.

Iwanari, M., Nakajima, M., Kizu, R., Hayakawa, K., and Yokoi, T. (2002). Induction of CYP1A1, CYP1A2, and CYP1B1 mRNAs by nitropolycyclic aromatic hydrocarbons in various human tissue-derived cells: Chemical-, cytochrome P450 isoform-, and cell-specific differences. *Arch. Toxicol.* **76,** 287–298.

Jonker, J. W., Smit, J. W., Brinkhuis, R. F., Maliepaard, M., Beijnen, J. H., Schellens, J. H., and Schinkel, AH. (2000). Role of breast cancer resistance protein in the bioavailability and fetal penetration of topotecan. *J. Natl. Cancer Inst.* **92,** 1651–1656.

Karim, A., Kook, C., Zitzewitz, D. J., Zagarella, J., Doherty, M., and Campion, J. (1976). Species differences in the metabolism and disposition of spironolactone. *Drug Metab. Dispos.* **4,** 547–555.

Katoh, M., Matsui, T., Nakajima, M., Tateno, C., Kataoka, M., Soeno, Y., Horie, T., Iwasaki, K., Yoshizato, K., and Yokoi, T. (2004). Expression of human cytochromes P450 in chimeric mice with humanized liver. *Drug Metab. Dispos.* **32,** 1402–1410.

Katoh, M., Matsui, T., Nakajima, M., Tateno, C., Soeno, Y., Horie, T., Iwasaki, K., Yoshizato, K., and Yokoi, T. (2005a). In vivo induction of human cytochrome P450 enzymes expressed in chimeric mice with humanized liver. *Drug Metab. Dispos.* **33,** 754–763.

Katoh, M., Matsui, T., Okumura, H., Nakajima, M., Nishimura, M., Naito, S., Tateno, C., Yoshizato, K., and Yokoi, T. (2005b). Expression of human phase II enzymes in chimeric mice with humanized liver. *Drug Metab. Dispos.* **33,** 1333–1340.

Katoh, M., Watanabe, M., Tabata, T., Sato, Y., Nakajima, M., Nishimura, M., Naito, S., Tateno, C., Iwasaki, K., Yoshizato, K., *et al.* (2005c). In vivo induction of human cytochrome P450 3A4 by rifabutin in chimeric mice with humanized liver. *Xenobiotica* **35,** 863–875.

Ko, H., Novak, E., Peters, G. R., Bothwell, W. M., Hosley, J. D., Closson, S. K., and Adams, W. J. (1989). Pharmacokinetics of single-dose cefmetazole following intramuscular administration of cefmetazole sodium to healthy male volunteers. *Antimicrob. Agents Chemother.* **33,** 508–512.

Kolis, S. J., Williams, T. H., and Schwartz, M. A. (1976). Identification of the urinary metabolites of ^{14}C-bumetanide in the rat and their excretion by rats and dogs. *Drug Metab. Dispos.* **4,** 169–176.

Murakawa, T., Sakamoto, H., Fukada, S., Nakamoto, S., Hirose, T., Itoh, N., and Nishida, M. (1980). Pharmacokinetics of ceftizoxime in animals after parenteral dosing. *Antimicrob. Agents Chemother.* **17,** 157–164.

Nishimura, M., Yoshitsugu, H., Yokoi, T., Tateno, C., Kataoka, M., Horie, T., Yoshizato, K., and Naito, S. (2005). Evaluation of mRNA expression of human drug-metabolizing enzymes and transporters in chimeric mouse with humanized liver. *Xenobiotica* **35,** 877–890.

Ohashi, R., Kamikozawa, Y., Sugiura, M., Fukuda, H., Yabuuchi, H., and Tamai, I. (2006). Effect of P-glycoprotein on intestinal absorption and brain penetration of antiallergic agent bepotastine besilate. *Drug Metab. Dispos.* **34,** 793–799.

Shimano, K., Satake, M., Okaya, A., Kitanaka, J., Kitanaka, N., Takemura, M., Sakagami, M., Terada, N., and Tsujimura, T. (2003). Hepatic oval cells have the side population phenotype defined by expression of ATP-binding cassette transporter ABCG2/BCRP1. *Am. J. Pathol.* **163,** 3–9.

Tanaka, Y., Sekiguchi, M., Sawamoto, T., Katami, Y., Ueda, T., Esumi, Y., and Noda, K. (1992). Absorption, distribution and excretion of zenarestat, a new aldose reductase inhibitor, in rats and dogs. *Xenobiotica* **22,** 57–64.

Tateno, C., Yoshizane, Y., Saito, N., Kataoka, M., Utoh, R., Yamasaki, C., Tachibana, A., Soeno, Y., Asahina, K., Hino, H., *et al.* (2004). Near completely humanized liver in mice shows human-type metabolic responses to drugs. *Am. J. Pathol.* **165,** 901–912.

Tsuda-Tsukimoto, M., Ogasawara, Y., and Kume, T. (2005). Pharmacokinetics and metabolism of TR-14035, a novel antagonist of a4ss1/a4ss7 integrin mediated cell adhesion, in rat and dog. *Xenobiotica* **35,** 373–389.

Welage, L. S., Borin, M. T., Wilton, J. H., Hejmanowski, L. G., Wels, P. B., and Schentag, J. J. (1990). Comparative evaluation of the pharmacokinetics of *N*-methylthiotetrazole following administration of cefoperazone, cefotetan, and cefmetazole. *Antimicrob. Agents Chemother.* **34,** 2369–2374.

Yamazaki, M., Neway, W. E., Ohe, T., Chen, I., Rowe, J. F., Hochman, J. H., Chiba, M., and Lin, J. H. (2001). In vitro substrate identification studies for P-glycoprotein-mediated transport: Species difference and predictability of in vivo results. *J. Pharmacol. Exp. Ther.* **296,** 723–735.

GH enhances proliferation of human hepatocytes grafted into immunodeficient mice with damaged liver

Norio Masumoto[1,2], Chise Tateno[1,3], Asato Tachibana[1,4], Rie Utoh[1], Yoshio Morikawa[4], Takashi Shimada[4], Hiroyuki Momisako[1,2], Toshiyuki Itamoto[2], Toshimasa Asahara[2,3] and Katsutoshi Yoshizato[1,3,5]

[1]Yoshizato Project, Cooperative Link of Unique Science and Technology for Economy Revitalization, Hiroshima Prefectural Institute of Industrial Science and Technology, 3-10-32 Kagamiyama, Higashihiroshima, Hiroshima 739-0046, Japan

[2]Division of Frontier Medical Science, Department of Surgery, Graduate School of Biomedical Sciences, Hiroshima University, 1-2-3 Kasumi, Minami-ku, Hiroshima 734-8551, Japan

[3]Hiroshima University Liver Project Research Center, 1-2-3 Kasumi, Minami-ku, Hiroshima 734-8551, Japan

[4]PhoenixBio Co. Ltd, 3-4-1 Kagamiyama, Higashihiroshima, Hiroshima 739-0046, Japan

[5]Developmental Biology Laboratory and Hiroshima University 21st Century COE Program for Advanced Radiation Casualty Medicine, Department of Biological Science, Graduate School of Science, Hiroshima University, 1-3-1 Kagamiyama, Higashihiroshima, Hiroshima 739-8526, Japan

(Correspondence should be addressed to K Yoshizato; Email: katsutoshi.yoshizato@phoenixbio.co.jp)

(C Tateno and K Yoshizato are now at PhoenixBio Co. Ltd, 3-4-1 Kagamiyama, Higashihiroshima, Hiroshima 739-0046, Japan)

(R Utoh is now at Institute of Advanced Life and Medical Sciences, Tokyo Women's Medical College, Kawada-chou 8-6, Shinjuku-ku, Tokyo 162-8666, Japan)

Abstract

We investigated effects of human (*h*) GH on the proliferation of *h*-hepatocytes that had been engrafted in the liver of albumin enhancer/promoter driven-urokinase plasminogen activator transgenic/severe combined immunodeficiency disease (uPA/SCID) mice (chimeric mice). The *h*-hepatocytes therein were considered to be deficient in GH, because *h*GH receptor (*h*GHR) is unresponsive to mouse GH. Actually, *h*IGF-1 was undetectable in chimeric mouse sera. The uPA/SCID mice were transplanted with *h*-hepatocytes from a 6-year (6Y)-old donor, and were injected with recombinant *h*GH (r*h*GH). r*h*GH stimulated the repopulation speed of *h*-hepatocytes; and up-regulated *h*IGF-1, human signal transducers and activators of transcription (*h*STAT) 3, and cell cycle regulatory genes such as human forkhead box M1, human cell division cycle 25A, and human cyclin D1. To confirm the reproducibility of these effects of r*h*GH, similar experiments were run using *h*-hepatocytes from a 46-year (46Y)-old donor. r*h*GH similarly enhanced their repopulation speed and up-regulated the expression of the above-tested genes, especially *h*IGF-1 and *h*STAT1. The extent of the enhancement by r*h*GH was much less than that in 6Y-hepatocyte-chimeric mice most probably due to the difference in GHR expression levels between the two donors. In conclusion, this study clearly demonstrated that r*h*GH stimulates the proliferation of *h*-hepatocytes *in vivo*.

Journal of Endocrinology (2007) **194**, 529–537

Introduction

Using rodents as experimental animals, it has been shown that differentiated hepatocytes can re-enter into the cell cycle when stimulated by growth factors, cytokines, and hormones (Taub 1996, Michalopoulos & DeFrances 1997, Fausto 2000). Hepatocytes in culture usually lose their replication ability and normal phenotypes and, thus, have had limited usability in testing the effects of these factors on hepatocytes. In addition, their effects on human (*h*)-hepatocytes *in vivo* have not been studied due to the lack of a suitable animal model. Previously, we developed a method to yield humanized mice (chimeric mice) whose liver is mostly replaced with *h*-hepatocytes (Tateno *et al.* 2004). The *h*-hepatocytes were transplanted into immunodeficient mice with diseased liver, albumin enhancer/promoter driven-urokinase plasminogen activator transgenic/severe combined immunodeficiency disease (uPA/SCID) mice. The transplanted cells were engrafted in the liver, continuously replicated, and repopulated in the liver. The extent of repopulation was calculated as the ratio (replacement index, RI) of the *h*-hepatocyte-repopulated area to the total examined area. Recent technological improvements enabled us to yield children's hepatocyte-chimeric mice with RI>96%. The chimeric mice have been proven to be a useful animal model to examine biological and pathological features of *h*-hepatocytes *in vivo* (Tateno *et al.* 2004, Tsuge *et al.* 2005).

The regeneration capacity of rat liver decreases with age (Bucher *et al.* 1964, Stocker & Heine 1971), which is coincident with the fact that serum concentrations of growth

Journal of Endocrinology (2007) **194**, 529–537
0022-0795/07/0194-529
DOI: 10.1677/JOE-07-0126
Online version via http://www.endocrinology-journals.org

hormone (GH) and insulin-like growth factor 1 (IGF-1) diminish with age (Kelijman 1991, Corpas *et al.* 1993), suggesting the association of GH with liver regeneration. Actually, evidence has been accumulating that GH is involved in liver regeneration and accounts for an aspect of age-dependent regenerative response of the liver in rodents (Krupczak-Hollis *et al.* 2003). However, the effects of GH on the growth of *h*-hepatocytes have not been studied *in vivo* at all yet. *h*GH is capable of stimulating rodent cells, whereas rodent GH cannot stimulate human cells because of its disability to bind to *h*GH receptors (*h*GHRs; Souza *et al.* 1995). Furthermore, it should be noted that *h*GH is not circulating in *h*-hepatocyte-chimeric mice, which indicates that *h*-hepatocytes in chimeric mice are in GH-deficient conditions. These facts and considerations strongly suggest that a chimeric mouse will provide an opportunity to examine the effects of *h*GH on growth of *h*-hepatocytes *in vivo*.

In this study, we examined the effects of *h*GH on the proliferation of *h*-hepatocytes using chimeric mice. The treatment of chimeric mice with *h*GH increased the repopulation speed and RI of transplanted *h*-hepatocytes, and up-regulated the GH-related signaling molecules. The present study shows that a *h*-hepatocyte-chimeric uPA/SCID mouse is a useful *in vivo* model to examine the effects of growth factors, cytokines, and hormones on *h*-hepatocytes.

Materials and Methods

Animals

The uPA/SCID mice weighing 6·3–10·0 g were produced as previously described (Tateno *et al.* 2004). The zygosity of the *uPA* transgene was determined by a multiplex PCR as previously described (Meuleman *et al.* 2003). Homozygous uPA/SCID mice were used as hosts throughout this study.

Transplantation of hepatocytes and bromodeoxyuridine (BrdU)-labeling

Cryopreserved *h*-hepatocytes from a 6-year-old Caucasian girl (6YG) and 46-year-old Caucasian man (46YM) respectively were purchased from *In vitro* Technologies (Baltimore, MD, USA) and thawed as previously described (Tateno *et al.* 2004). Trypan blue-exclusion test showed that the viability of 6YG- and 46YM-hepatocytes was 71·5±4·3% ($n=3$) and 72·2±2·3% ($n=3$) respectively. The *h*-hepatocytes (7·5 or $10·0\times10^5$ viable cells) were transplanted into the inferior splenic pole of uPA/SCID mice at 20–30 days after birth, through a small left-flank incision (Tateno *et al.* 2004). BrdU (Sigma Chemical Co.) was intraperitoneally injected into chimeric mice at a dose of 50 mg/kg body weight at 1 h before killing. Histological sections were prepared from the liver and stained with anti-BrdU antibodies as described below.

rhGH treatment

The 6YG- and 46YM-hepatocyte-chimeric mice were divided into two groups at 1 day post-transplantation; recombinant *h*GH (*rh*GH; Wako Pure Chemical Industries Ltd, Osaka, Japan)-treated ($rhGH^+$, experimental) and -untreated ($rhGH^-$, control) groups. *rh*GH was dissolved in water and used for animal injection. Animals of experimental groups were daily administered from day 1 after transplantation to 1 day before the day of killing with *rh*GH by subcutaneous injection at 2·5 μg/10 μl per g body weight.

Measurement of human albumin (hAlb) and human IGF-1 concentrations in mouse blood or sera

*h*Alb concentration in blood of a chimeric mouse is correlated with RI of transplanted hepatocytes (Tateno *et al.* 2004). Blood (2 μl) was collected from the tail vein of *h*-hepatocyte-chimeric mice. The blood *h*Alb concentrations were determined with a latex agglutination assay (Eiken Immunochemical Laboratory, Tokyo, Japan) or a *h*Alb ELISA quantitation kit (Bethyl Laboratories Inc., Montgomery, TX, USA). As a measure of GH/IGF-1 signaling in the chimeric mice, serum human IGF-1 (*h*IGF-1) concentrations were determined using a *h*IGF-I ELISA kit (R&D Systems Inc., Minneapolis, MN, USA).

Immunohistochemistry and measurement of RI

Frozen sections were prepared from chimeric livers, fixed in −20 °C acetone for 5 min and incubated with anti-human cytokeratin 8 and 18 (*h*CK8/18) antibodies (dilution, 1:25; MP Biomedicals, Aurora, OH, USA). The *h*CK8/18 antibodies reacted with *h*-hepatocytes but not with mouse (*m*)-hepatocytes. Formalin-fixed paraffin sections of chimeric livers were incubated with mouse anti-BrdU antibodies (dilution, 1:10; DakoCytomation, Glostrup, Denmark) and goat anti-*h*Alb antibodies (dilution, 1:1000; Bethyl Laboratories). The primary antibodies were visualized with a Vectastain ABC kit (Vector Laboratories, Burlingame, CA, USA) or peroxidase- and dextran-conjugated anti-mouse immunoglobulins (Dako Envision +; DakoCytomation) with 3, 3′-diaminobenzidine (Sigma) as substrates. The sections were counterstained with Mayer's hematoxylin. RI was calculated as the ratio of area occupied by *h*CK8/18-positive hepatocytes to the entire area examined on immunohistochemical sections of six lobes (Tateno *et al.* 2004). The ratios of BrdU-positive nuclei to *h*Alb-positive *h*-hepatocytes were determined by counting at least 1000 cells in 10 to 15 randomly selected vision fields in sections.

Quantification of mRNA in the livers of chimeric mice

Total RNAs were purified from liver tissues by an RNeasy mini kit (Qiagen). Using 1 μg total RNA by PowerScript reverse transcriptase (Clontech Inc.) and Random Primer oligonucleotides (Invitrogen Corp.), cDNAs were

synthesized according to the manufacturer's instruction. The mRNAs of genes shown in Table 1 were quantified in the liver tissues of chimeric mice by real-time RT-PCR (Tateno *et al.* 2004). Genes were amplified with a set of gene-specific primers shown in Table 1 and SYBR Green PCR mix (Applied Biosystems, Tokyo, Japan) in PRISM 7700 Sequence Detector (Applied Biosystems). We confirmed that these primers for *h*-genes amplified the *h*- but not the *m*-genes. Real-time RT-PCR was performed as follows: initial denaturation step at 95 °C for 10 min, followed by 40 cycles at 95 °C for 15 s and 60 or 62 °C for 1 min. All data were treated as previously described (Livak & Schmittgen 2001). The expression levels of the tested genes were normalized to the expression level of human glyceraldehyde 3-phosphate dehydrogenase (*hGAPDH*) gene and human hypoxanthine phosphoribosyltransferase 1 (*hHPRT-1*) gene.

Statistical analysis

Data were analyzed with StatView, 5.0 (SAS Institute Inc., Cary, NC, USA). Results are shown as the mean ± S.E.M. or S.D., and the significance of the difference between two groups under comparison was analyzed by Student's *t*-test when data were normally distributed and otherwise by Welch's test.

Results

Relationship of engraftment with repopulation of h-*hepatocytes*

In this study, we aimed to quantitatively assess the effect of r*h*GH on the extent of repopulation of *h*-hepatocytes in chimeric mice. It was considered that the number of engrafted *h*-hepatocytes depends on the number of the injected cells and affects the time length to reach the final (maximal) RI. Thus, we first examined the relationship between the number of the originally engrafted *h*-hepatocytes and that of the maximally repopulated *h*-hepatocytes, assuming that there is a linear relationship between the occupancy rate of *h*-hepatocytes after transplantation and the number of originally engrafted *h*-hepatocytes before the occupancy rate reaches the maximum when the repopulating *h*-hepatocytes terminate the proliferation (the saturation phase of the repopulation). Ten and 27 uPA/SCID mice were transplanted with 7·5 and $10{\cdot}0\times10^5$ 6YG-hepatocytes/animal respectively. All of the animals were successfully engrafted with *h*-hepatocytes. Blood *h*Alb levels were determined at 19–22 days post-transplantation as a measure of the number of the originally engrafted *h*-hepatocytes, and at 55–61 days as a measure of the number of the repopulated *h*-hepatocytes. The levels of '19–22 day'-group ($h\text{Alb}_{19\text{–}22}$) are plotted against those of '55–61 day'-group ($h\text{Alb}_{55\text{–}61}$; Fig. 1). The graph consisted of two regions, a near linear region in which $h\text{Alb}_{55\text{–}61}$ increased with $h\text{Alb}_{19\text{–}22}$ in a near linear fashion and a region of near plateau in which the increase of $h\text{Alb}_{19\text{–}22}$ did not meaningfully increase $h\text{Alb}_{55\text{–}61}$. It can be said that the plateau level (6–10 mg/ml) represented the maximal level (the maximal RI) of the occupancy of *h*-hepatocytes in the experimental conditions we adopted. In the case of $7{\cdot}5\times10^5$ cell transplantation, most chimeric mice showed $h\text{Alb}_{19\text{–}22}<0{\cdot}5$ mg/ml, and $h\text{Alb}_{55\text{–}61}$ was increased with the increase of $h\text{Alb}_{19\text{–}22}$. This result supported the above assumption that *h*-hepatocytes near lineally increased in number with the increase in the number of the originally engrafted *h*-hepatocytes and they did not reach the maximal repopulation state until 55–61 days post-transplantation. However, it should be noted here that the *h*Alb level does not correctly reflect the number of the repopulated *h*-hepatocytes as we showed in the previous study (Tateno *et al.* 2004) and also in the present study.

In contrast, in the case of $10{\cdot}0\times10^5$ cell transplantation, most of the chimeric mice showed $h\text{Alb}_{19\text{–}22}>0{\cdot}5$ mg/ml and reached the plateau level (>6 mg/ml) at 55–61 days, suggesting that there is an appropriate number of *h*-hepatocytes to be injected to obtain a high-engraftment rate (the number ratio of the engrafted *h*-hepatocytes to the injected *h*-hepatocytes). It is considered that the number of $7{\cdot}5\times10^5$ was smaller than this appropriate number. It appeared in $10{\cdot}0\times10^5$*h*-hepatocyte transplantation experiments that the proliferation of

Table 1 Oligonucleotide primers used in PCR amplification of growth hormone (GH)-related genes

Gene	Forward primer (5′–3′)	Reverse primer (5′–3′)
hGHR	TCACTCAAGGTTGAATCACAC	TCACATCAAGGTTGAATCACAC
hIGF-I	GCTTCCGGAGCTGTGATCTAA	GCTGACTTGGCAGGCTTG
hSTAT1	TTGCAGAACAGAGAACACGAGA	CATTCTGGGTAAGTTCAGTGAC
hSTAT3	GACCAACAATCCCAAGAATGTA	AATAATTCACACCAGGTCCCAA
hFoxM1	GCATCTACTGCCTCCCTGTG	GAGGAGTCTGCTGGGAACG
hCdc25A	CAAAGAGGAGGAAGAGCATGTC	CCAGGGATAAAGACTGATGAAGAG
hcyclin B1	CCTGATGGAACTAACTATGTTG	CATGTGCTTTGTAAGTCCTTGA
hcyclin D1	TGTGAAGTTCATTTCCAATCCG	CTGGAGAGGAAGCGTGTGAG
hCdk1	AAACTACAGGTCAAGTGG	GGGATAGAATCCAAGTATTTCTTCAG
hCdk2	ACAAGTTGACGGGAGAGGTG	CAGAAATTCAAAAACCAGGTAGAGT
hGAPDH	CCACCTTTGACGCTGGG	CATACCAGGAAATGAGCTTGACA
hHPRT1	TGGTCAGGCAGTATAATC	CAGTTTAGGAATGCAGCA

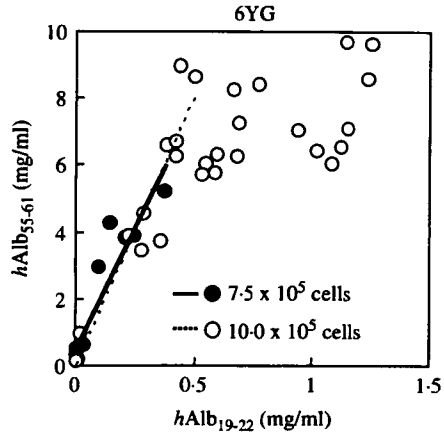

Figure 1 Relationship between *h*Alb concentrations in early and late time points after transplantation. uPA/SCID mice were transplanted with 7·5 (closed circles) and $10{\cdot}0\times10^5$ 6YG-hepatocytes (open circles). *h*Alb levels at 19–22 days post-transplantation ($h\text{Alb}_{19\text{–}22}$) were plotted against those at 55–61 days ($h\text{Alb}_{55\text{–}61}$). The $h\text{Alb}_{55\text{–}61}$ in the $7{\cdot}5\times10^5$ cell-transplantation experiment were lineally correlated with those at the $h\text{Alb}_{19\text{–}22}$ ($r^2=0{\cdot}86$, solid line). The $h\text{Alb}_{55\text{–}61}$ in the $10{\cdot}0\times10^5$ cell-transplantation experiment were also lineally correlated with $h\text{Alb}_{19\text{–}22}$ in the range <0·5 mg/ml of *h*Alb ($r^2=0{\cdot}87$, dotted line).

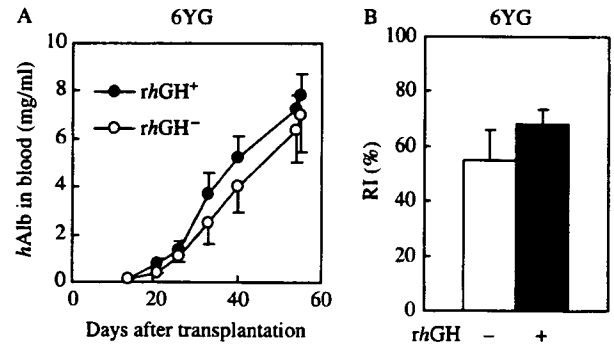

Figure 2 Repopulation of *h*-hepatocytes in uPA/SCID mice. Each uPA/SCID mouse was transplanted with $10{\cdot}0\times10^5$ 6YG-hepatocytes. Animals in $rh\text{GH}^+$ group were daily injected with *rh*GH and *h*Alb concentrations in host blood were monitored (A). RIs of $rh\text{GH}^-$ (open bar)- and $rh\text{GH}^+$ 6YG-chimeric mice (closed bar) were determined at 55 days post-transplantation (B). Values represent the mean±S.E.M. of three different mice.

h-hepatocytes terminated around 60 days post-transplantation when the *h*Alb level reached 6 mg/ml irrespective of $h\text{Alb}_{19\text{–}22}$, probably due to the contact inhibition among the *h*-hepatocytes, the toxicity of *h*-hepatocytes for the mouse when *h*Alb exceeded 6 mg/ml, and other yet unknown reasons. In $10{\cdot}0\times10^5$ cell-transplantation experiments, there were several mice that showed $h\text{Alb}_{19\text{–}22}<0{\cdot}5$ mg/ml. An apparent similar relationship between $h\text{Alb}_{19\text{–}22}$ and $h\text{Alb}_{55\text{–}61}$ was seen in these animals as in $7{\cdot}5\times10^5$ *h*-hepatocyte transplantation experiments. Therefore, we empirically concluded that *h*-hepatocytes increased in number in an apparently quasilinear fashion after the engraftment from $h\text{Alb}_{19\text{–}22}<0{\cdot}5$ mg/ml to $h\text{Alb}_{55\text{–}61}<6$ mg/ml. Thus, we utilized chimeric mice with $h\text{Alb}_{19\text{–}22}<0{\cdot}5$ mg/ml for examining the effects of *h*GH on the proliferation of *h*-hepatocytes in the following experiments.

It has been generally recognized that *h*GH is capable of stimulating rodent cells, whereas rodent GHs are not able to bind to GHRs on *h*-hepatocytes (Souza *et al.* 1995). Six uPA/SCID mice were transplanted with $10{\cdot}0\times10^5$ 6YG-hepatocytes/mouse. Half of them were treated with *rh*GH. The blood *h*Alb levels were monitored throughout the experimental period (up to 55 days) after transplantation (Fig. 2A). The concentrations of *h*Alb rapidly increased and exceeded 0·5 mg/ml (0·5–1·36 mg/ml) around 20 days post-transplantation in all mice irrespective of the treatment of *rh*GH and reached over 6 mg/ml around 50 days after transplantation. There were no differences in *h*Alb levels between $rh\text{GH}^-$ and $rh\text{GH}^+$ chimeric mice. At the end of this experiment, mice were killed for determining RI on immunohistological sections prepared from their liver tissues (Fig. 2B). Also, there were no differences in RIs between the two groups. Serum *h*IGF-1 levels were determined for mice from $rh\text{GH}^-$ and $rh\text{GH}^+$ groups. *h*IGF-1 was not detected in the animals of $rh\text{GH}^-$ groups whose *h*Alb concentrations were 8·2±1·1 mg/ml ($n=3$). In contrast *h*IGF-1 was detectable (11·9±11·2 mg/ml, $n=3$) in mice of $rh\text{GH}^+$ groups whose *h*Alb concentrations were 7·9±1·9 mg/ml ($n=3$). Thus, the absence of *h*IGF-1 in sera of mice in $rh\text{GH}^-$ groups is explainable at least in part by assuming that *h*-hepatocytes did not respond to *m*GH in the chimeric mice, and when *rh*GH was given, *h*-hepatocytes responded to it and up-regulated *h*IGF-1 expression.

Enhancement of the repopulation of h*-hepatocytes by hGH*

Nine and eight uPA/SCID mice were transplanted with $7{\cdot}5\times10^5$ 6YG- and $10{\cdot}0\times10^5$ 46YM-hepatocytes/animal, then five and four of them were treated with *rh*GH respectively. Chimeric mice with both 6YG- and 46YM-hepatocytes showed variable *h*Alb levels, which were 0·01–0·6 and 0·0005–0·3 mg/ml at 20 days post-transplantation respectively. Three $rh\text{GH}^+$ and $rh\text{GH}^-$ mice with 0·01–0·05 mg/ml *h*Alb each were selected from 6YG- and 46YM-chimeric mice. The *rh*GH enhanced the increase of *h*Alb levels in both groups (Fig. 3). $rh\text{GH}^-$ animals slowly increased the values after 20 days post-transplantation, whereas $rh\text{GH}^+$ mice rapidly increased them in 6YG-chimeric mice (Fig. 3A). The transplanted cells in $rh\text{GH}^-$ 46YM-mice also slowly grew as in 6YG-mice (Fig. 3B). The *rh*GH also accelerated the repopulation in these mice, though its effect was considerably lower when compared with 6YG-hepatocyte mice.

The chimeric mice transplanted with 6YG- and 46YM-hepatocytes shown in Fig. 3A and B respectively were killed at 70 and 76 days post-transplantation for histological examinations respectively. There were no differences between $rh\text{GH}^+$ and $rh\text{GH}^-$ mice in body weight and liver size at the time of killing. *h*-Hepatocytes were immunohistochemically identified as *h*CK8/18-positive cells (Fig. 3C through F). Distributions of the immunopositive 6YG- and 46YM-cells in $rh\text{GH}^-$ animals are shown in Fig. 3C and E respectively. *h*-Hepatocyte colony

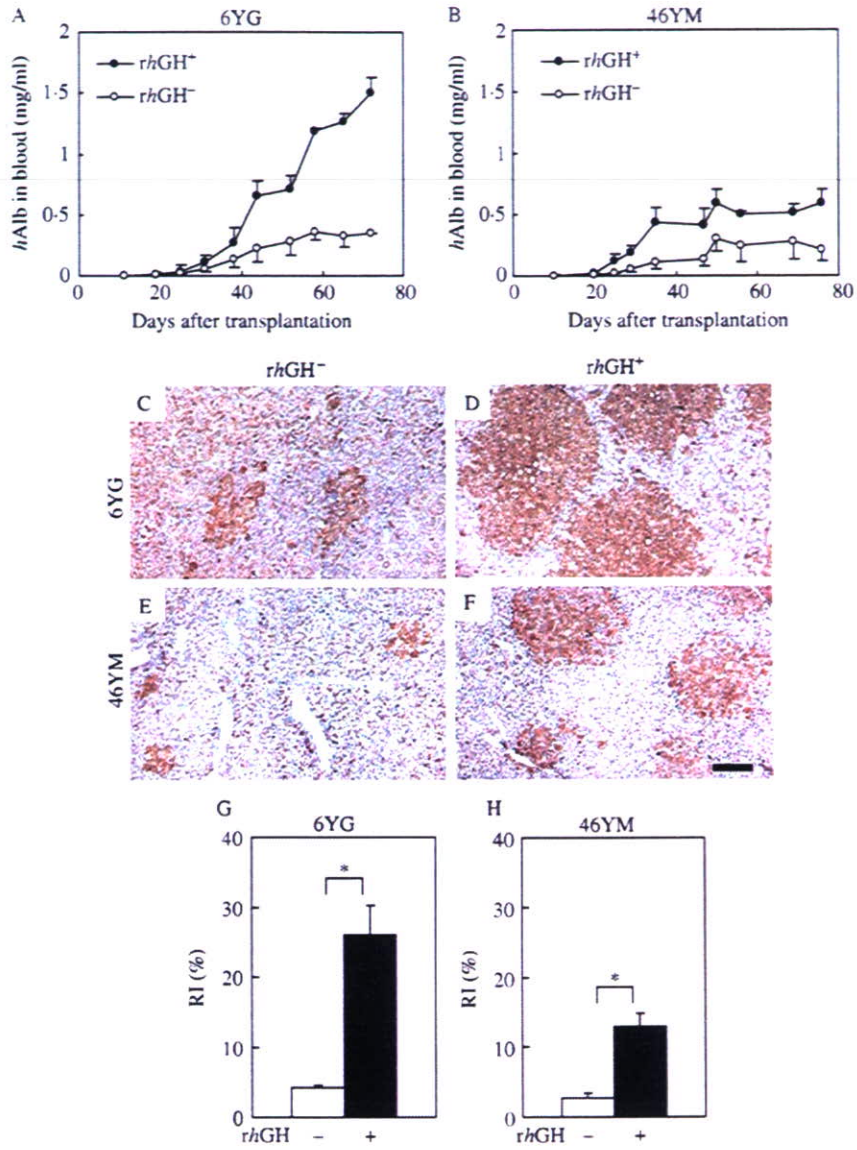

Figure 3 Effects of *h*GH on repopulation of *h*-hepatocytes. 6YG ($7{\cdot}5\times10^5$, A)- and 46YM ($10{\cdot}0\times10^5$, B)-hepatocytes were transplanted into each of uPA/SCIDmice and treated with r*h*GH as in Fig. 2. *h* Alb concentrations were monitored once a week. Solid and open circles show r*h*GH$^+$ and r*h*GH$^-$ mice respectively (C through F). Histological sections were prepared from six liver lobes of 6YG-chimeric mice at 70 days post-transplantation (C and D) and from those of 46YM-chimeric mice at 76 days post-transplantation (E and F). The sections were stained with anti-*h*CK8/18 antibodies. Sections 'C and E' and 'D and F' were from r*h*GH$^-$ and r*h*GH$^+$ mice respectively. The cytoplasm of hCK8/18-positive *h*-hepatocytes is stained brown. Scale bar in F: 20 μm (C and H). RI was calculated as the ratio of the brown colored areas to the examined total ones for 6YG- (G) and 46YM-chimeric mice (H). Open and closed bars show r*h*GH$^-$and r*h*GH$^+$ mice respectively. Values represent the mean±S.E.M. of three different mice. Asterisks indicate significant differences ($^*P<0{\cdot}05$, Student's *t*-test).

sizes were larger in 6YG- than in 46YM-hepatocytes. The size was greatly increased in r*h*GH$^+$ mice for both 6YG- (Fig. 3D) and 46YM-hepatocytes (Fig. 3F). *h*GH increased RI ~6·2- and 4·8-fold in 6YG-and 46YM-hepatocyte-chimeric mice respectively (Fig. 3G and H).

Effects of r*h*GH *on DNA synthesis of* h*-hepatocytes in chimeric mice*

We investigated whether r*h*GH stimulated the DNA synthesis of *h*-hepatocytes in chimeric mice. uPA/SCID mice were transplanted with 6YG- or 46YM-hepatocytes, injected with

*r*hGH, and were exposed with BrdU before killing at 2 weeks post-transplantation. BrdU-positive *h*-hepatocytes were often distributed in the peripheral regions of the colonies (Fig. 4A for 6YG-hepatocytes). The BrdU-labeling index of 6YG-hepatocytes in *r*hGH$^+$ mice was 2·2-fold higher ($P<0·05$) than that in *r*hGH$^-$ mice (Fig. 4B), indicating that GH induced the entry of *h*-hepatocytes into the S-phase of the cell cycle. The index of *r*hGH$^+$ 46YM-mice was 1·4-fold higher than that of *r*hGH$^-$ ones, but the difference was not significant.

Expression of hepatocyte growth-associated genes in chimeric livers

Previously, we showed the BrdU-labeling index of *h*-hepatocytes (9-month-old Caucasian boy) in chimeric mice at 1, 3, and 5 weeks post-transplantation was ~9, 5, and 2% respectively, and thereafter gradually decreased to <0·5% at 10–11 weeks (Emoto *et al.* 2005). Taking the present results shown in Fig. 4 and the above cited previous ones together, we considered that transplanted *h*-hepatocytes become most proliferative around 1 week post-transplantation, and, thus, hepatocyte growth-associated genes become activated then. However, there were not enough *h*-hepatocytes yet to yield sufficient RT-PCR amplification. Thus, we examined the effect of *r*hGH on the expression of hepatocyte growth-associated genes in *h*-hepatocytes of chimeric livers at 2 weeks point post-transplantation. Chimeric mice were treated with *r*hGH as in Fig. 4 and were killed at 2 weeks post-transplantation to determine mRNA levels of 10 genes by real-time RT-PCR: *h*GHR, *h*IGF-1, human signal transducers and activators of transcription (*h*STAT) 1, *h*STAT3, human forkhead box (*h*Fox) M1, human cell division cycle (*h*Cdc) 25A, *h*-cyclin B1, *h*-cyclin D1, human cyclin-dependent kinases (*h*Cdk) 1, and *hCdk2*. The expression levels were normalized to that of *hGAPDH* gene. The ratios of the expression under *r*hGH$^+$ to that under *r*hGH$^-$ are depicted as graphs for 6YG- (Fig. 5A) and 46YM-mice (Fig. 5B). *r*hGH did markedly increase *h*IGF-1 mRNA in both 6YG- (Fig. 5A) and 46YM-hepatocyte-chimeric mice (Fig. 5B; $P<0·05$, Student's *t*-test or Welch's test). The stimulation rate (9·1-fold) in 6YG-hepatocyte mice was much higher than that (2·6-fold) in 46YM-hepatocyte ones. The effects of *r*hGH were generally much prominent in chimeric mice bearing 6YG-hepatocytes as compared with that in those bearing 46YM-ones. In 6YG-hepatocyte-chimeric mice, *r*hGH significantly increased the expressions of mRNAs of *h*STAT3, *h*FoxM1, *h*Cdc25A, and *h*-cyclin D1 ($P<0·05$, Student's *t*-test, Fig. 5A). The expression levels for mRNAs of *h*STAT1, *h*-cyclin B1, *h*Cdk1, and *h*Cdk2 were higher in the *r*hGH$^+$- group than in *r*hGH$^-$ group in 6YG-hepatocyte-chimeric mice, although the difference in the ratio between the two groups was not significant. Similarly, mRNAs of *h*STAT1 and *h*STAT3 were induced by *r*hGH in 46YM-hepatocyte-chimeric mice, although the difference was not significant (Fig. 5B). In contrast to the expression in 6YG-chimeric mice, *r*hGH did not induce mRNAs of *h*FoxM1, *h*Cdc25A, *h*-cyclin B1, *h*-cyclin D1, *h*Cdk1, and *h*Cdk2 in 46YM-chimeric mice (Fig. 5B). 6YG-hepatocytes expressed *h*GHR mRNA at a 19·5-fold higher level than 46YM-hepatocytes in *r*hGH$^-$ group, suggesting differences in the responsiveness of these growth-related genes to *rhGH* might be due to the difference in GHR expression levels between the two donors. Similar results were obtained when the data were normalized by *h*HPRT-1 as another housekeeping gene.

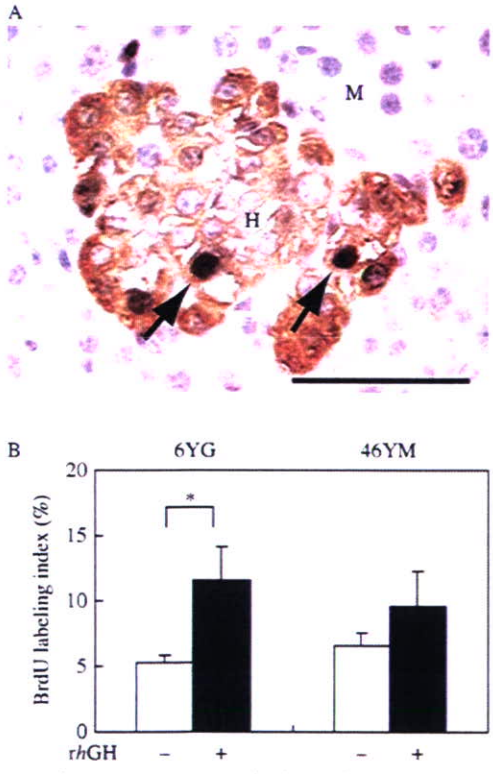

Figure 4 BrdU incorporation in the liver of chimeric mice. 6YG- and 46YM-hepatocytes were transplanted into uPA/SCIDmice, and they were treated with *r*hGH as in Fig. 2. They were injected with BrdU at 2 weeks post-transplantation, and killed 1 h later. A. The liver sections from a 6YG-chimeric mouse were subjected to double immunostaining with BrdU and *h*Alb. *h*Alb-positve *h*-hepatocytes have brown cytoplasm. BrdU-positive *h*-hepatocytes have dark brown nuclei (arrows). M and H indicate regions of *m*- and *h*-hepatocytes. Scale bar: 50 μm. B. BrdU-labeling index was calculated as the ratio of BrdU-positive nuclei to all the counted nuclei. Solid and open bars show *r*hGH$^+$ and *r*hGH$^-$ mice respectively. Values represent the mean±S.D. of experiments with 6YG- mice ($n=3$) and 46YM-mice ($n=4$). Asterisks indicate significant differences at * $P<0·05$ (Student's *t*-test).

Discussion

Hepatocytes of uPA/SCID mice undergo severe injury and, thus, genes of cytokines involved in liver regeneration are activated (Mars *et al.* 1995, Michalopoulos & DeFrances

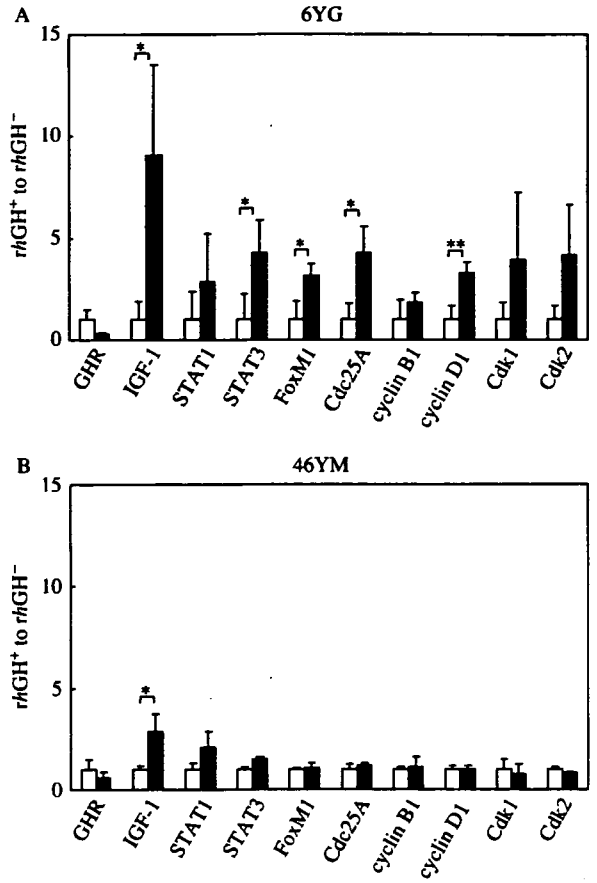

Figure 5 Expression of GH-related genes in chimeric mouse liver. Chimeric mice were yielded by transplanting 6YG- (A) and 46YM-hepatocytes (B), and treated with *rh*GH as in Fig. 2. The animals were killed at 2 weeks after transplantation. RNA was extracted from livers and used for determining the amount of mRNAs of ten genes, *h*GHR, *h*IGF-1, *h*STAT1, *h*STAT3, *h*FoxM1, *h*Cdc25A, *h*-cyclin B1, *h*-cyclin D1, *h*Cdk1, *h*Cdk2, and *h*GAPGH by real-time quantitative RT-PCR. Each data was divided by the data of *h*GAPDH. The graphs represent the ratio of the *rh*GH$^+$ to the *rh*GH$^-$ levels. Open and closed bars show *rh*GH$^-$ and *rh*GH$^+$ mice respectively. Values represent the mean±S.D. Asterisks indicate significant differences at $^*P<0.05$ and $^{**}P<0.01$.

1997). GH is one of such stimulators of liver regeneration in rodents (Krupczak-Hollis *et al.* 2003, Pennisi *et al.* 2004). Krupczak-Hollis *et al.* (2003) showed that GH promoted the proliferation of hepatocytes upon the partial hepatectomy in mice, which was mediated through activation of *FoxM1B* gene. Transgenic mice bearing GH-antagonist genes showed an incomplete liver regeneration and a reduced renewal rate of hepatocytes (Pennisi *et al.* 2004), suggesting a critical role of GH in liver regeneration. Regeneration-associated proliferation of hepatocytes in mice was impaired with a liver-specific IGF-1 receptor gene knockout (Desbois-Mouthon *et al.* 2006). In contrast to such abundant studies on rodents, there have been no studies on the effects of GH on *h*-hepatocytes *in vivo*. We undertook the present study assuming that a chimeric mouse will provide an opportunity to examine the effects of *rh*GH on proliferation of *h*-hepatocytes *in vivo*, because we considered that *h*-hepatocytes in chimeric mice are in GH-deficient conditions. This consideration was supported by the present study because we showed that *h*IGF-1 was actually undetectable in the chimeric mouse sera. We expected that *rh*GH treatment might enhance the proliferation of *h*-hepatocytes in uPA/SCID mice. Chimeric mice were yielded bearing *h*-hepatocytes from two donors whose sex and age were different, 6YG and 46YM, and were treated with *rh*GH. As a result, we were able to demonstrate for the first time that *rh*GH stimulates the proliferation of *h*-hepatocytes *in vivo*. This conclusion was reproducibly obtained from the two independent experiments using hepatocytes from different donors, although the extent of the stimulation was much higher for 6YG-hepatocytes than for 46YM-hepatocytes. This difference of GH-stimulation between the two donors might be explainable by the difference of GHR-expression level between them as shown in this study.

Studies on the molecular mechanisms of the action of GH are currently progressing in rodents. *c-fos* gene is an immediate early responsive gene to GH, which is mediated by STAT1 and STAT3 (Gronowski & Rotwein 1994, Gronowski *et al.* 1995, Herrington *et al.* 2000). Our study showed that *rh*GH increased the expression of *h*STAT1 and *h*STAT3 mRNAs in *h*-hepatocytes in chimeric mice. GH stimulates the growth of target cells through GHRs and its endocrine IGF-1 (Daughaday & Rotwein 1989). GH stimulates the synthesis and the secretion of IGF-1 by hepatocytes (Sjogren *et al.* 1999, Yakar *et al.* 1999). Secreted IGF-1 binds to the IGF-IR, which activates the expression of cell cycle-related genes such as cyclin D1 through ERK pathway (Desbois-Mouthon *et al.* 2006). Our present study showed that *rh*GH enhanced the expression of *h*IGF-I and cyclin D1 mRNAs in the liver of chimeric mice. Therefore, it is concluded that GH stimulates the growth of *h*-hepatocytes through activating GH/IGF-I/IGF-IR/ERK signaling. These results suggest that the stimulation of growth of hepatocytes by GH is induced through similar mechanisms in both rodents and humans. Studies remain to be done on the protein phosphorylation or the activation of the signaling cascades after the *rh*GH-stimulation using currently developed *h*-hepatocyte-chimeric mice.

It was shown in rodents that GH increases the FoxM1 level (Krupczak-Hollis *et al.* 2003), which stimulates the cell cycle progression at both the G1/S- and G2/M-phase transitions (Wang *et al.* 2001, 2002*a*,*b*, 2005, Major *et al.* 2004). Progression through the cell cycle is regulated by the temporal activation of multiple families of Cdk. Cdc25A, Cdc25B, and Cdc25C with phosphatase activities are involved in the activation of Cdks in a way that these enzymes dephosphorylate catalytic units of Cdks (Sebastian *et al.* 1993). Upon S-phase progression, Cdc25A phosphatase activates Cdk2-cyclin E by dephosphorylating inhibitory Cdk2 residues (Massague 2004). Progression through the

G2/M transition requires the activation of the Cdk1-cyclin B complex through dephosphorylation and the activation of Cdk1 by the Cdc25B and Cdc25C phosphatases, the latter of which is activated by Polo-like kinase 1 phosphorylation (Barr *et al.* 2004). It is noteworthy that *rh*GH up-regulated mRNAs of *h*FoxM1, *h*Cdc25A, *h*-cyclin B1, *h*-cyclin D1, *h*Cdk1, and *h*Cdk2 in 6YG-hepatocytes, but not 46YM-counterparts. Thus, it can be said that GH activates cell cycle progression of *h*-hepatocytes as known in rodents. The phosphorylation levels of Janus activating kinase 2 and GHR complex were decreased with age of rats (Xu *et al.* 1995). In the present study we showed that 6YG-hepatocytes expressed *h*GHR mRNA at much higher levels than 46YM-hepatocytes. This apparent age-dependent GH-expression level of *h*-hepatocytes should be tested in further studies with sufficient samples of donor hepatocytes for statistical treatments of the obtained results.

In this study we demonstrated usefulness of a *h*-hepatocyte-chimeric uPA/SCID mouse as an *in vivo* model to study effects of GH on the proliferation of *h*-hepatocytes. *h*-Hepatocyte-chimeric mice were also yielded using another type of immunodeficient and liver-injured mice obtained by crossing uPA-transgenic mice with mice whose recombinant activation gene-2 (RAG-2) had been deleted (Dandri *et al.*, 2001). It is worthy of examining in the future whether the effects of *rh*GH on *h*-hepatocytes observed in the present study can be reproduced in this uPA/RAG-2 mouse model. As clearly demonstrated for GH–GHR binding in the present study, *h*-hepatocytes in mice could be deficient for other growth factors and cytokines due to problems in interspecies ligand–receptor interaction. However, this limitation of *h*-hepatocyte-chimeric mice will provide us opportunities to study the mechanism of their interactions *in vivo* using chimeric mice in place of human body as exemplified for *rh*GH on *h*-hepatocytes in this study.

Acknowledgements

This study was supported by Cooperative Link of Unique Science and Technology for Economy Revitalization, Japan. We thank Y Yoshizane, H Kohno, Y Matsumoto, and S Nagai for breeding the mice and providing excellent technical assistance. The authors declare that there is no conflict of interest that would prejudice the impartiality of this scientific work.

References

Barr FA, Sillje HH & Nigg EA 2004 Polo-like kinases and the orchestration of cell division. *Nature Reviews. Molecular Cell Biology* **5** 429–440.

Bucher NL, Swaffield MN & DiTroia JF 1964 The influence of age upon the incorporation of thymidine-2-C14 into the DNA of regenerating rat liver. *Cancer Research* **24** 509–512.

Corpas E, Harman SM & Blackman MR 1993 Human growth hormone and human aging. *Endocrine Reviews* **14** 20–39.

Dandri M, Burda MR, Torok E, Pollok JM, Iwanska A, Sommer G, Rogiers X, Rogler CE, Gupta S, Will H *et al.* 2001 Repopulation of mouse liver with human hepatocytes and *in vivo* infection with hepatitis B virus. *Hepatology* **33** 1005–1006.

Daughaday WH & Rotwein P 1989 Insulin-like growth factors I and II. Peptide, messenger ribonucleic acid and gene structures, serum, and tissue concentrations. *Endocrine Reviews* **10** 68–91.

Desbois-Mouthon C, Wendum D, Cadoret A, Rey C, Leneuve P, Blaise A, Housset C, Tronche F, Le Bouc Y & Holzenberger M 2006 Hepatocyte proliferation during liver regeneration is impaired in mice with liver-specific IGF-1R knockout. *FASEB Journal* **20** 773–775.

Emoto K, Tateno C, Hino H, Amano H, Imaoka Y, Asahina K, Asahara T & Yoshizato K 2005 Efficient *in vivo* xenogeneic retroviral vector-mediated gene transduction into human hepatocytes. *Human Gene Therapy* **16** 1168–1174.

Fausto N 2000 Liver regeneration. *Journal of Hepatology* **32** 19–31.

Gronowski AM & Rotwein P 1994 Rapid changes in nuclear protein tyrosine phosphorylation after growth hormone treatment *in vivo*. *Journal of Biological Chemistry* **269** 7874–7878.

Gronowski AM, Zhonq Z, Wen Z, Thomas MJ, Darnell JE Jr & Rotwein P 1995 *In vivo* growth hormone treatment rapidly stimulates the tyrosine phosphorylation and activation of Stat3. *Molecular Endocrinology* **9** 171–177.

Herrington J, Smit LS, Schwartz J & Carter-Su C 2000 The role of STAT proteins in growth hormone signaling. *Oncogene* **19** 2585–2597.

Kelijman M 1991 Age-related alterations of the growth hormone/insulin-like-growth-factor I axis. *Journal of the American Geriatrics Society* **39** 295–307.

Krupczak-Hollis K, Wang X, Dennewitz MB & Costa RH 2003 Growth hormone stimulates proliferation of old-aged regenerating liver through Forkhead Box m1b. *Hepatology* **38** 1552–1562.

Livak KJ & Schmittgen TD 2001 Analysis of relative gene expression data using real-time quantitative PCR and the $2^{-\Delta\Delta C_T}$ method. *Methods* **25** 402–408.

Major ML, Lepe R & Costa RH 2004 Forkhead Box M1B (FoxM1B) transcriptional activity requires binding of Cdk/cyclin complexes for phosphorylation-dependent recruitment of p300/CBP co-activators. *Molecular and Cellular Biology* **24** 2649–2661.

Mars WM, Liu ML, Kitson RP, Goldfarb RH, Gabauer MK & Michalopoulos GK 1995 Immediate early detection of urokinase receptor after partial hepatectomy and its implications for initiation of liver regeneration. *Hepatology* **21** 1695–1701.

Massague J 2004 G1 cell-cycle control and cancer. *Nature* **432** 298–306.

Meuleman P, Vanlandschoot P & Leroux-Roels G 2003 A simple and rapid method to determine the zygosity of uPA-transgenic SCID mice. *Biochemical and Biophysical Research Communications* **308** 375–378.

Michalopoulos GK & DeFrances MC 1997 Liver regeneration. *Science* **276** 60–66.

Pennisi PA, Kopchick JJ, Thorgeirsson S, LeRoith D & Yakar S 2004 Role of growth hormone (GH) in liver regeneration. *Endocrinology* **145** 4748–4755.

Sebastian B, Kakizuka A & Hunter T 1993 Cdc25M2 activation of cyclin-dependent kinases by dephosphorylation of threonine-14 and tyrosine-15. *PNAS* **90** 3521–3524.

Sjogren K, Liu JL, Blad K, Skrtic S, Vidal O, Wallenius V, LeRoith D, Tornell J, Isaksson OG, Jansson JO *et al.* 1999 Liver-derived insulin-like growth factor I (IGF-I) is the principal source of IGF-I in blood but is not required for postnatal body growth in mice. *PNAS* **96** 7088–7092.

Souza SC, Frick GP, Wang X, Kopchick JJ, Lobo RB & Goodman HM 1995 A single arginine residue determines species specificity of the human growth hormone receptor. *PNAS* **92** 959–963.

Stocker E & Heine WD 1971 Regeneration of liver parenchyma under normal and pathological conditions. *Beiträge zur Pathologie* **144** 400–408.

Tateno C, Yoshizane Y, Saito N, Kataoka M, Utoh R, Yamasaki C, Tachibana A, Soeno Y, Asahina K, Hino H *et al.* 2004 Near completely humanized liver in mice shows human-type metabolic responses to drugs. *American Journal of Pathology* **165** 901–912.

Taub R 1996 Liver regeneration 4: transcriptional control of liver regeneration. *FASEB Journal* **10** 413–427.

Tsuge M, Hiraga N, Takaishi H, Noguchi C, Oga H, Imamura M, Takahashi S, Iwao E, Fujimoto Y, Ochi H *et al.* 2005 Infection of human hepatocyte chimeric mouse with genetically engineered hepatitis B virus. *Hepatology* **42** 1046–1054.

Wang X, Quail E, Hung NJ, Tan Y, Ye H & Costa RH 2001 Increased levels of Forkhead box M1B transcription factor in transgenic mouse hepatocytes prevent age-related proliferation defects in regenerating liver. *PNAS* **98** 11468–11473.

Wang X, Kiyokawa H, Dennewitz MB & Costa RH 2002*a* The Forkhead Box M1B transcription factor is essential for hepatocyte DNA replication and mitosis during mouse liver regeneration. *PNAS* **99** 16881–16886.

Wang X, Krupczak-Hollis K, Tan Y, Dennewitz MB, Adami GR & Costa RH 2002*b* Increased hepatic Forkhead Box M1B (FoxM1B) levels in old-aged mice stimulated liver regeneration through diminished $p27^{Kip1}$ protein levels and increased Cdc25B expression. *Journal of Biological Chemistry* **277** 44310–44316.

Wang IC, Chen YJ, Hughes D, Petrovic V, Major ML, Park HJ, Tan Y, Ackerson T & Costa RH 2005 Forkhead Box M1 regulates the transcriptional network of genes essential for mitotic progression and genes encoding the SCF (Skp2-Cks1) ubiquitin ligase. *Molecular and Cellular Biology* **25** 10875–10894.

Xu X, Bennett SA, Ingram RL & Sonntag WE 1995 Decreases in growth hormone receptor signal transduction contribute to the decline in insulin-like growth factor I gene expression with age. *Endocrinology* **136** 4551–4557.

Yakar S, Liu JL, Stannard B, Butler A, Accili D, Sauer B & LeRoith D 1999 Normal growth and development in the absence of hepatic insulin-like growth factor I. *PNAS* **96** 7324–7329.

Received in final form 3 June 2007
Accepted 7 June 2007
Made available online as an Accepted Preprint
12 June 2007

Cytometry
PART A

Single Lymphocyte Analysis with a Microwell Array Chip

Yoshiharu Tokimitsu,[1,2] Hiroyuki Kishi,[1*] Sachiko Kondo,[1] Ritsu Honda,[1] Kazuto Tajiri,[1,2] Kazumi Motoki,[1] Tatsuhiko Ozawa,[1] Shinichi Kadowaki,[1] Tsutomu Obata,[3] Satoshi Fujiki,[3] Chise Tateno,[4] Hideki Takaishi,[5] Kazuaki Chayama,[5] Katsutoshi Yoshizato,[6] Eiichi Tamiya,[7] Toshiro Sugiyama,[2] Atsushi Muraguchi[1]

[1]Department of Immunology, Graduate School of Medicine and Pharmaceutical Sciences, University of Toyama, Toyama, Japan

[2]The Third Department of Internal Medicine, Graduate School of Medicine and Pharmaceutical Sciences, University of Toyama, Toyama, Japan

[3]The Central Institute, Toyama Industrial Technology Center, Takaoka, Toyama, Japan

[4]The Yoshizato Project, CLUSTER, Hiroshima Prefectural Institute of Industrial Science and Technology, Higashi-Hiroshima, Japan

[5]Department of Medicine and Molecular Science, Division of Frontier Medical Science, Graduate School of Biomedical Sciences, Hiroshima University, Hiroshima, Japan

[6]Developmental Biology Laboratory, Department of Biological Science, Graduate School of Science, Hiroshima University, Higashi-Hiroshima, Japan

[7]Department of Applied Physics, Osaka University, Suita, Osaka, Japan

*Correspondence to: Hiroyuki Kishi; Department of Immunology; Graduate School of Medicine and Pharmaceutical Sciences; University of Toyama, 2630 Sugitani, Toyama 930-0194, Japan

Email: immkishi@med.u-toyama.ac.jp

Published online 30 October 2007 in Wiley InterScience (www.interscience.wiley.com)

DOI: 10.1002/cyto.a.20478

• Abstract

Following genomics and proteomics, cytomics, a novel method of looking at life, has emerged for analyzing large populations of cells on a single-cell basis with multiple parameters in a quantitative manner. We have developed a highly integrated live-cell microarray system for analyzing the cellular responses of individual cells using a microwell array chip that has 234,000 microwells each of which is just large enough to fit a single cell. Compared with flow cytometry and microscope-based methods, our system can analyze the history of the cellular responses of a large number of cells. We have successfully applied the system to analyze human antigen-specific B-cells and produced human monoclonal antibodies (MoAb) against hepatitis B virus surface antigen. We have also constructed a mouse system to assess hepatitis B virus-neutralization activity and have demonstrated the neutralization activity of our antibodies. Our technology should expand the horizons of cell analysis as well as enable generation of human MoAb for antibody-based therapeutics and diagnosis for infectious diseases such as hepatitis viruses.

• Key terms

lymphocyte; microwell array chip; monoclonal antibody; hepatitis B virus; intracellular calcium

CYTOMICS is a novel perspective from which to look at life and to study the "cytome," analyzing large populations of cells on a single-cell basis with multiple parameters in a quantitative and observer-independent manner (1). To meet the discipline of cytomics, sensitive fluorescence detection devices and sophisticated image analysis procedures have been developed, including tools based on flow cytometry or those based on microscopy (2). Flow cytometers have enabled us to analyze fluorescent signals of large numbers of cells flowing through sheath fluid, but they cannot track the history of the fluorescent signals from each cell of interest. In contrast, tools based on microscopes have enabled us to analyze signals of individual cells at various time points. However, we cannot analyze a large number of cells with a microscope, especially when cells are nonadherent.

B-cells, a major cell population in immune systems, produce antibodies that specifically recognize antigens, such as infectious microbes, neutralize their infectivity, and eliminate them by various immune effector mechanisms. B-cells express mono-specific antibodies on the cell surface as antigen receptors that recognize extra-cellular antigens. It has been estimated that an individual human contains on the order of 10^7 clones of B-cells with distinct specificities (3). It has also been reported that the frequencies of antigen-specific B-cells are quite diverse, which may be due to the form of immunogen. For example, more than 10% of B-cells produce

This article contains supplementary material available via the Internet at http://www.interscience.wiley.com/jpages/1552-4922/suppmat.

Received 14 March 2007; Revision Received 19 July 2007; Accepted 11 September 2007

Grant sponsors: Toyama Medical Bio-Cluster Project, Hiroshima Bio-Cluster Project of the Ministry of Education, Culture, Sports, Science and Technology, Japan

the specific antibodies to rabies (4), but only 0.01% of B-cells produce antibodies to hepatitis B virus surface (HBs) antigen (HBs-Ag) after vaccination (5). To analyze the response of individual B-cells to an antigen, it is necessary to analyze a large number of cells at the level of a single cell by cytomics.

To meet the demand for this type of analysis, we have developed an analysis system using a microwell array chip that has a large number of microwells whose size and shape just fit a single cell (6). By applying an individual cell to each microwell, an array of live cells was prepared, and the cellular responses of individual cells, such as alteration of intracellular Ca^{2+} concentration, were monitored using a fluorescent scanner that was modified to scan cells. Because the position of each cell was fixed, we could repeatedly analyze the cellular response of the same cell. Consequently, a cell microarray system, a combination of a microwell array chip and a cell scanner, enabled us to analyze the time course of the cellular responses of a large number of cells at the single-cell level. Recently, Deutsch et al. (7) and Biran and Walt (8) reported live cell arrays for analyzing a large number of cells at the single-cell level. These cell arrays were chiefly designed for analyzing cells, and the retrieval of objective cells from wells without disturbing surrounding cells might be difficult. In contrast, our cell microarray system was aimed at not only analyzing cells but also retrieving objective cells from an array.

Hepatitis B virus (HBV) infection is one of the world's major health problems, especially in East Asia. It causes self-limiting acute hepatitis, but the infection may often become chronic, causing hepatic cirrhosis and hepatic cell cancer. Vaccines based on recombinant DNA technology have been developed and applied for the protective immunization of humans. Such vaccination, however, does not always provoke a sufficient and rapid antibody response, and HB immunoglobulins (HBIg) have been employed in combination with HB vaccination (9). HBIg injection, however, poses some serious problems such as contamination by unknown infectious agents and lack of a continuous supply in hospitals. Human monoclonal antibodies (MoAb) represent an alternative to HBIg therapy.

We have applied our cell microarray system to detect human B-cells that respond to HBs-Ag from the peripheral blood of HBs-Ag-vaccinated volunteers, and obtained HBs-Ag-specific MoAb that neutralized HBV to prevent its infection of human hepatocytes. Our technology may contribute to the production of human MoAb not only for HBV but also for other various human health-threatening infectious agents, such as AIDS and SARS as well as microbes that might be used for bioterrorism.

Materials and Methods

Microwell Array Chip

A microwell array chip was manufactured using micromachining (microelectromechanical system) techniques (10) (Supplementary Fig. 1). Briefly, a thin film of silicon dioxide was grown on a silicon surface by thermal oxidation (11), a photoresist was coated on the thin film, and microwell patterns were transferred from a mask via photolithography using a Karl Suss MA6 Mask Aligner (SUSS MicroTec AG, Garching, Germany). Then, the exposed oxidized silicon surface was etched by silicon deep reactive ion etching (12) to form microwells using buffered hydrofluoric acid as a solvent of silicon dioxide. Then, a fluorocarbon polymer was formed on the photoresist and the sidewall of a microwell using plasma-enhanced chemical vapor deposition (13). Finally, the photoresist was removed and the fluorocarbon polymer was lifted off the surface of the silicon chip.

Preparation of Lymphocytes for Intracellular Calcium Analysis

To analyze the efficiency of the cell microarray system, we used splenocytes of MD4 transgenic mice (C57BL/6-Tg(IghelMD4)4Ccg/J from The Jackson Laboratory, Bar Harbor, ME), of which the transgene encodes mouse antibody (HyHEL10) for hen egg lysozyme (HEL) (14). The splenocytes were prepared and loaded with 0.1 μM CellTracker orange (Ex, 535 nm; Em, 585 nm; Invitrogen, Carlsbad, CA) and 0.1 μM Fluo-4 (Ca^{2+}-dependent fluorophore; Ex, 473 nm; Em, 532 nm; Invitrogen), as previously described (6). The procedure for the transgenic mice experiments was approved by the Committee for Recombinant DNA Experiments (#19-9) and Animal Experiments at the University of Toyama (# 2006-Med-33). The mice were examined to determine whether they were transgenic by staining peripheral blood lymphocytes with biotinylated HEL and PE-conjugate of streptavidin. The mice with HEL-specific Ab-expressing B-cells were used for the experiments.

For preparation of human B-cells, peripheral blood lymphocytes were isolated from healthy donors according to the standard Ficoll–Hypaque method (Lymphosepal; IBL, Takasaki, Japan). B-cells were purified using MACS (Miltenyi Biotec K.K., Tokyo, Japan), and loaded with CellTracker orange and Fluo-4.

Cell Microarray Analysis and Antibody Preparation

Cell microarray analysis was performed as previously described (6). Briefly, cells were loaded onto a microwell array

chip and the Fluo-4 fluorescence of the individual cells before stimulation was measured by scanning the chip with a cell scanner (CRBIO IIe-FITC, Hitachi Software, Tokyo, Japan) that was modified from a DNA chip scanner (CRBIO IIe) by changing a 635-nm laser to a 473-nm laser and whose minimum resolution was improved to 2.5 μm. The cells were then stimulated with antigen at room temperature in air by exchanging the buffer on the chip with buffer containing antigen, and the cellular Fluo-4 fluorescence was measured with the scanner after stimulation. The Fluo-4 fluorescence intensities of the individual cells before and after antigen-stimulation were plotted in a scatter diagram with TIC-Chip Analysis software (Hitachi Software). Cells whose fluorescence increased more than fivefold were retrieved as antigen-activated B-cells from each well with a micromanipulator (TransferMan NK2, Eppendorf, Hamburg, Germany). To prepare an antibody from a retrieved B-cell, antibody cDNA was amplified with single-cell RT-PCR, inserted into an expression vector, and transfected into 293T cells to obtain a supernatant containing the antibody as previously described (6) (see supplementary Fig. 2).

ELISA for Detection of Anti-HBs Antibody

Maxisorp 96-well plates (Nunc, Roskilde, Denmark) were coated with 50 μl/well of 10 μg/ml HBs-Ag (Kaketsuken, Kumamoto, Japan) in phosphate buffered saline (PBS) and then blocked with 3% casein in PBS. After washing, cell culture supernatant containing the antibody was added to the plates and incubated for 15 min at room temperature. The binding of human antibody to the coated antigen was detected using alkaline phosphatase-labeled anti-human immunoglobulins and *p*-nitrophenylphosphate. The optical absorbance was measured at 414 nm with an ELISA reader (Labsystem Japan, Tokyo, Japan). To confirm the antigen-specificity of an antibody, a competitive binding assay was performed. Briefly, in the ELISA assay described earlier, 0.4, 2.0, 10 μg/ml soluble HBs-Ag was added together with the culture supernatants that contained the anti-HBs antibody.

Estimation of the Epitope

For the estimation of the anti-HBs antibody epitope, competitive ELISA was performed with mouse anti-HBs MoAb (anti-d, Institute of Immunology, Takasaki, Japan; anti-a and anti-r, provided from T. Nakashima, Kaketsuken) whose epitopes were already determined. Briefly, to Maxisorp 96-well plates coated and blocked as described earlier was added 50 μl/well of diluted mouse anti-HBs MoAb as a competitor, followed by 50 μl/well of 20 ng/ml sample antibody. After 15-min incubation at room temperature, binding of the sample antibody was assessed as described earlier.

In Vivo Neutralizing Activity Assay

To examine the HBV neutralization activity of the antibodies, chimeric mice having human hepatocytes were used. The chimeric mice were produced by transplanting human hepatocytes into albumin enhancer/promoter-driven urokinase-type plasminogen activator-transgenic SCID mice (uPA/SCID mice) (15). The transplanted human hepatocytes were shown to be infected with hepatitis C virus and HBV (16,17). Human serum albumin produced from the transplanted human hepatocytes was in the range of 1.3–5.2 mg/ml, indicating that 32–66% of the liver cells were replaced with those of human origin. Serum of a chronic hepatitis B patient was used for the preparation of HBV. The titer of the virus was determined by quantitative PCR of the virus genome as previously described (16). Primers for PCR are listed in supplementary Table 1. For the test of neutralization activity, the patient serum that contained 1.0×10^6 copies of the virus was mixed with 30 μg of either control or anti-HBs antibodies, incubated at room temperature for 30 min, and then intravenously injected into mice. For the estimation of neutralization activity, virus titers in the sera of the infected mice were measured every 2 weeks as described earlier.

Results

A Live Cell Microarray System for Lymphocytes

A general view of the live cell microarray system that we have developed is shown in Figure 1A. The cell suspension is prepared from blood or tissue, and loaded with fluorophore whose intensity alters with cell conditions, such as Ca^{2+} concentration, membrane potential, and pH. Then, the live cells are applied onto the microwell array chip that contains an array of 234,000 wells in which only a single cell can be trapped. Cells are stimulated with or without stimulants such as infectious reagents, and the alteration in fluorescence is monitored with a cell scanner. The signal of each cell is analyzed on a single-cell basis. Because the position of each cell on the chip is fixed, the signal of any one cell can be repeatedly analyzed. Then, individual cells of interest are identified, retrieved, analyzed at the molecular level, and used for protein engineering.

To prepare a live cell microwell array chip for lymphocytes, we manufactured a microwell array chip as shown in supplementary Figure 1. The microwell array chip was fabricated on a silicon substrate by using a micromachining technique (10). A scanning electron micrograph of the chip is shown in Figure 1B. To smoothly apply single cells to and retrieve them from the microwells, we made the surface of the microwell array chip hydrophilic by growing silicon dioxide using a thermal oxidation process (11), and the bottom and the sidewall hydrophobic by coating with a thin fluorocarbon film. To prepare the live lymphocyte array, the lymphocytes were separated, loaded with fluorescent dye, and applied to the microwell array chip. The chip was covered with a cover glass to prevent drying. The array of the live lymphocytes was examined under a fluorescence microscope (Fig. 1C). To raise the array rate and to efficiently hold the single lymphocytes in the microwells, the sizes (diameter and depth) as well as shapes of the microwells were optimized (Fig. 1D and data not shown). When the depth of the microwells is less than 10 μm, the lymphocytes in the microwells were easily moved out during a washing step. As a result, cylindrical microwells with a diameter of 10 μm and a depth of more than 12 μm were most suitable for raising the array rate and efficiently holding the

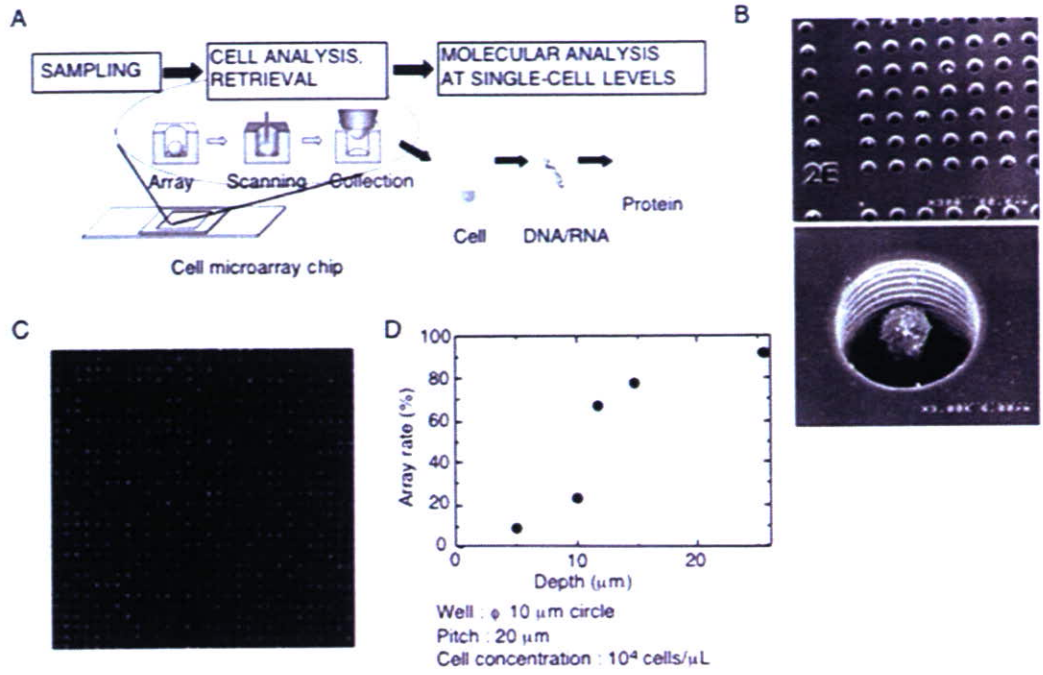

Figure 1. A cell microarray system. (**A**) General view of the cell microarray system. Lymphocytes are spread in the microwell array chip and their cellular responses are monitored. The responding cells are then retrieved and used for molecular analysis and protein engineering at the single-cell level. (**B**) Scanning electron micrograph images. Wide view (top) and single-well view (bottom) are shown. The lymphocyte became smaller due to the fixation process. (**C**) Picture of live cell array. Lymphocytes are loaded with CellTracker orange, arrayed on the chip, and observed under a fluorescence microscope. (**D**) Relationship between well depth and cell array rate. 50 μl of 10^4 cells/μl lymphocytes is applied on a chip. The percentage of wells that trap lymphocytes after any untrapped cells are washed away is the array rate.

lymphocytes. The relationship between the spacing of the microwells and number of arrayed cells was also investigated. When the spaces between the microwells increased, the number of arrayed cells decreased (data not shown). Based on these data, a microwell array chip with wells at a pitch of 20 μm, a diameter of 10 μm, and a depth of 15 μm were used in the following experiment.

Detection of Antigen-Stimulated Activated B-Cells on the Chip, and Comparison of Efficiency with a Flow Cytometry System

We first assessed the efficiency of the cell microarray system using mouse B-cells prepared from MD4 mice that carry a transgene encoding antibody (HyHEL10) to HEL (14). It has been reported that when MD4 B-cells, which express HyHEL10 antibody on their cell surface, are stimulated with HEL, the cells are activated and their intracellular Ca^{2+} concentrations increase (18). We prepared MD4 B-cells, loaded them with a fluorescent Ca^{2+} indicator, Fluo-4 (19), and arrayed them on the chip. The fluorescence of the cells was monitored with a cell scanner that was equipped with a 473-nm laser to activate and monitor the fluorescence of Fluo-4. Before stimulation, the fluorescence of each cell was measured and analyzed with the cell scanner at the single-cell level (left panel of Fig. 2A). Then, MD4 splenocytes were stimulated with HEL and their fluorescence was monitored with the cell scanner (right panel of Fig. 2A). The cell scanner scans the total cell area between 30 and 90 s after the stimulation. Because the address of each cell on the chip is fixed, we could compare the fluorescence intensity of each cell before and after stimulation by using analysis software. As shown in Figure 2B, dots corresponding to cells whose fluorescence was unchanged after the stimulation were located on the "$y = x$" line. When B-cells were activated with HEL, the intracellular Ca^{2+} level was increased, and the fluorescence intensity was augmented by a factor of about five. Dots corresponding to such activated B-cells shifted upward and were discriminated from those of the unstimulated cells. If cells with a twofold increase in Fluo-4 fluorescence were considered as positive cells, 49% of the cells were positive. If cells with a fourfold increase in fluorescence were considered as positive cells, 17% of the cells became positive. The earlier results demonstrate that a combination of a microwell array chip and a cell scanner (cell microarray system) can monitor the activation of about 200,000 individual cells by monitoring the alteration of intracellular Ca^{2+} concentration. We then compared the efficiency of the cell microarray system for detection of activated MD4 B-cells with that of a flow cytometry system (Figs. 2B and 2C). Splenocytes prepared from MD4 transgenic mice or normal mice were prepared and loaded with Fluo-4. These cells were mixed

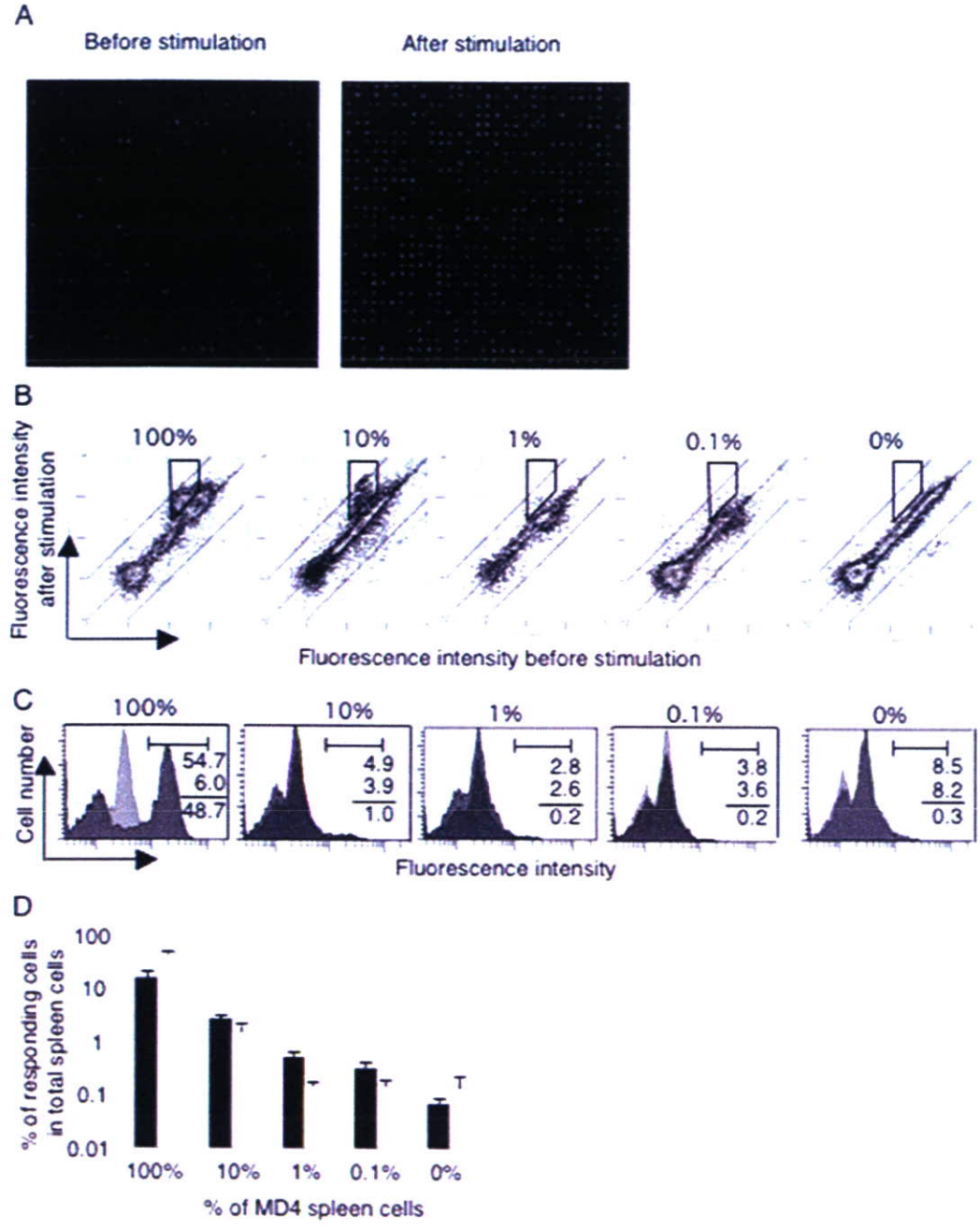

Figure 2. Analysis of B-cells with the cell microarray system. (**A**) Scanned image of intracellular Ca^{2+} signals of B-cells arrayed on a microwell array chip before and after stimulation. MD4 B-cells were loaded with Fluo-4, stimulated with HEL on the chip, and scanned with a cell scanner before (left) and after (right) stimulation. (**B**) Scattered plots of Fluo-4-intensities of MD4 B-cells before and after HEL-stimulation. Various percentages (100%, 10%, 1%, 0.1%, and 0%) of MD4 splenocytes were prepared by mixing with normal splenocytes, loaded with Fluo-4, arrayed on a chip, and stimulated with HEL (10 μg/ml). The cells were scanned with a cell scanner and Fluo-4 fluorescence signals before (*x*-axis) and after (*y*-axis) stimulation were calculated and plotted on scatter diagrams. Each spot corresponds to one cell. Cells whose fluorescence was not altered correspond to dots on the blue line ($y = x$). Dots of the activated cells shifted upward. Cells with more than a fourfold increase in Fluo-4 fluorescence intensity were considered as responding cells and enclosed with a box. (**C**) The same MD4 B-cell preparation was analyzed with a flow cytometer. Fluorescence histograms of lymphocytes before (light gray) and after (dark gray) stimulation are shown. The percentages of fluorescence positive cells after stimulation, before stimulation, and their differences are shown from top to bottom in each panel. (**D**) Comparison of cell microarray system and flow cytometry for detecting activated cells. The percentages of HEL-activated MD4 B-cells detected with either the cell microarray system (black column) or flow cytometry (open column) were calculated as in Figures 2B or 2C. The results represent the average of three independent experiments, and error bars represent the standard deviation.

with various ratios such as 100%, 10%, 1%, and 0.1% MD4 spleen cells. Cell preparation was applied on the microwell array chip and stimulated with HEL, and the fluorescence of each B-cell before and after stimulation with HEL was measured with the cell scanner (Fig. 2B). To compare the detection efficiency with flow cytometry, the spleen cell mixture was stimulated with HEL and the alteration of fluorescence intensity was also measured with a flow cytometer (Fig. 2C). Figure 2D shows the percentages of positively detected cells with the cell microarray system or flow cytometry. We selected cells with a more than fourfold increase in Fluo-4 fluorescence after stimulation with antigen as antigen-activated B-cells in the cell microarray analysis. For the flow cytometry analysis, we calculated the positive cells by subtracting the percentage of positive cells before stimulation from the percentage of positive cells after stimulation. As noted, we observed the cell population with high Fluo-4 fluorescence intensity before stimulation, which was detected not only in the cell microarray system but also in flow cytometry (Figs. 2A–2C). The cell microarray system could distinguish the false positive cells and antigen-stimulated cells whose Fluo-4 fluorescence signals increased after antigen stimulation because each cell address was fixed on the chip and the fluorescence levels of the same cell before and after stimulation could be compared. In contrast, flow cytometry could not make the same distinction because it could not repeatedly monitor the signals of specific cells. Therefore, the detection of antigen-stimulated B-cells of low frequency with flow cytometry was hampered by the false positive cells, but was not hampered with the cell microarray system (Fig. 2D). In the case of the microwell array chip, the percentage of positively detected cells was linearly decreased with the dilution of MD4 spleen cells and about 0.2% of the positive cells were still detected in 0.1% of the MD4 spleen cells. The background of the positive cells was around 0.08% (Figs. 2B and 2D). In contrast, an analysis of less than 1% of the MD4 spleen cells with the flow cytometry system could not show the difference because of the false positive cells (Figs. 2C and 2D).

Application to the Detection of HBV-Specific B-Cells and Generation of MoAb with Neutralizing Activity of HBV Infection

Because the efficacy of detecting single cells using the cell microarray system was verified, we tried to apply the system to detect human antigen-specific B-cells and prepare human antigen-specific MoAb. Volunteers were vaccinated with recombinant HBs-Ag according to the vaccination protocol. Seven days after the last vaccination, B-cells were prepared from peripheral blood, loaded with Fluo-4, applied on a microwell array chip, and stimulated with HBs-Ag on the chip. The fluorescence intensity of individual cells before and after stimulation was measured with the cell scanner. As shown in Figure 3A, the fluorescence intensity of the minor cell population increased with the HBs-Ag stimulation. Figure 3B shows the percentage of activated B-cells before and after the boost of HBs-Ag in the volunteers. The HBs-Ag boost almost doubled the percentage of positive cells (Fig. 3B). We then retrieved the positive cells from the microwells using a micro-

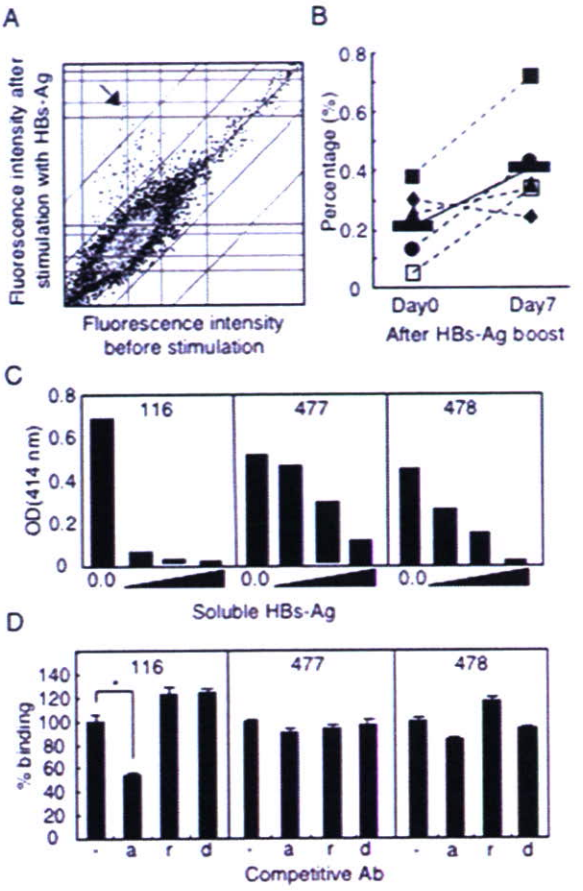

Figure 3. Detection of HBs-Ag-specific B-cells and production of HBs-Ag-specific antibodies with the cell microarray system. (**A**) Scatter diagram of peripheral blood B-cells before and after stimulation with HBs-Ag (100 μg/ml). (**B**) Percentage of HBs-Ag-stimulated B-cells in peripheral blood B-cells before and after application of HBs vaccine. Black bars show the average. (**C**) Antigen specificity of anti-HBs antibody. The antigen specificity of 116, 477, and 478 antibodies were examined with a competitive binding assay. Binding of the antibodies to plate-coated HBs-Ag was examined in the presence of various doses (0.4, 2, 10 μg/ml) of soluble HBs-Ag. Representative data of three to four independent experiments are shown. (**D**) Determination of epitope of anti-HBs antibodies. Binding of the antibodies to plate-coated HBs-Ag was examined in the presence of competitive MoAb to specific epitopes (a, r, d) on HBs-Ag. $^*P < 0.01$.

manipulator and the heavy chain and light chain variable regions of cDNA were augmented from a single B-cell by RT-PCR. The cDNAs were inserted into expression vectors, which were then cotransfected to 293T cells derived from human embryonic kidney (Supplementary Fig. 2). The culture supernatants of the 293T cells were collected and the specific binding activity of the antibody was analyzed with ELISA. Sixty-six IgM and 12 IgG cDNAs were cloned from 377 individual B-cells. In 12 IgG cDNAs, 3 IgG (116, 477, and 478) were found to bind HBs-Ag specifically (Fig. 3C). It has been reported

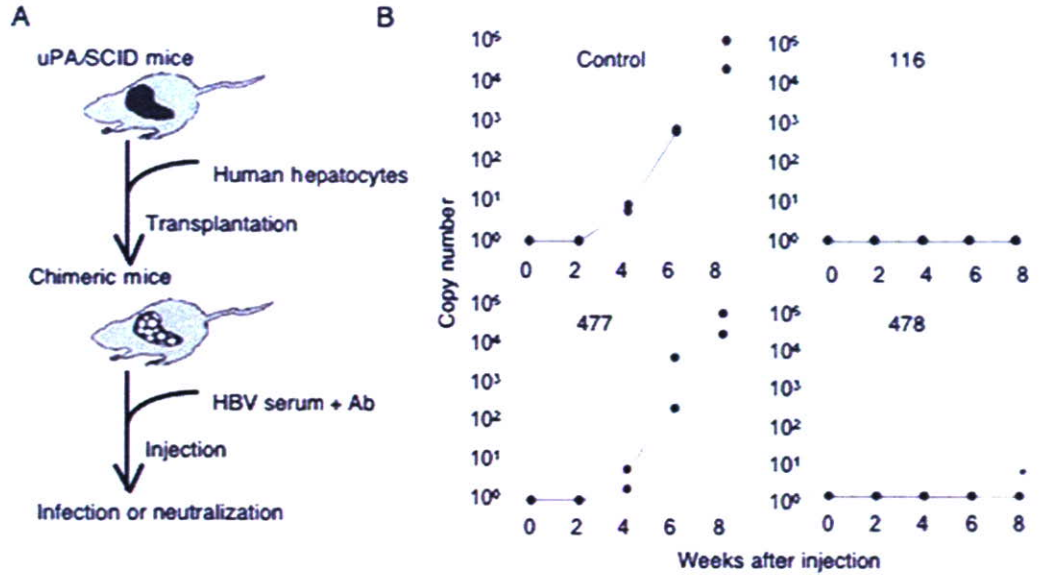

Figure 4. Assessment of virus neutralization activity of anti-HBs antibodies. (**A**) Scheme of protocol for examination of HBV neutralization activity with human hepatocyte-chimeric mice. (**B**) Effect of anti-HBs antibodies on HBV infection. A mixture of HBV and anti-HBs antibodies or control antibody was injected i.v. into human hepatocyte-chimeric mice, and the virus titer in mouse serum was determined by a quantitative viral genome PCR analysis ($n = 2$). *One mouse died during the 8-week study. Representative data of two independent experiments are shown.

that there are three major epitopes, a, d/y, and r/w on HBs-Ag (20). The epitopes recognized by the IgG antibodies were examined by competition with epitope-specific antibodies. As shown in Figure 3D, 116 was found to bind epitope "a" since the "a"-epitope-specific antibody inhibited the binding of 116 to HBs-Ag. Because the other antibodies (477 and 478) were not competed with the antibodies used, we could not determine their epitopes. The affinities of the 116, 477, and 478 antibodies were determined with surface plasmon resonance. It was revealed that their K_d were 1.2×10^{-9} M, 5.9×10^{-7} M, and 1.4×10^{-7} M, respectively (data not shown).

Finally, we tested to see if these antibodies inhibit the infection of HBV in human hepatocytes. We used chimeric mice to which human hepatocytes had been transplanted (16,17) (Fig. 4A). We injected i.v. 1.0×10^6 copies of HBV into the mice in the presence of control, 116, 477, or 478 antibody. Infection and replication of the virus was determined by detecting the viral genomic DNA in the serum with PCR. Figure 4B shows that the virus DNA was detected 4 weeks later in the chimeric mice injected with the virus together with either the control or 477 antibody. In contrast, the virus DNA was not detected in the serum of the mice that had been injected with the virus together with either the 116 or 478 antibody, demonstrating that these antibodies showed the neutralizing activity.

Discussion

We described a live cell microarray chip, which arrays a large number of nonadherent cells, such as lymphocytes, by accommodating them in microwells whose size and shape are optimized to trap only a single cell. By stimulating individual cells on the chip and monitoring cell signals such as intracellular Ca^{2+} levels before and after antigen-stimulation, we could efficiently detect the activation of individual cells. Since the cell scanner repeatedly scans 234,000 cells in about 2 min/scan, it can follow the history of cell signals every 2 min. We verified that this system is more suitable for analyzing the "cytome" (21,22) when compared with microscopy and flow cytometry-based systems, which cannot analyze the history of the cellular responses of large numbers of cells at the level of single cells. Using a novel microwell array chip, we could successfully analyze human B-cells of volunteers who had been vaccinated with HBs-Ag and generate some MoAb that were able to neutralize the HBV infection of human hepatocytes.

Regarding the viability of cells on the chip, Fluo-4 fluorescence intensities of about 90% of the B-cells were increased by stimulation with anti-IgM antibodies (data not shown). As about 90% of B-cells express IgM on the cell surface, the result indicates that most of the B-cells were alive on the chip during the assay. The diameter and depth of the microwells were critical in preparing an array of single cells (data not shown and Fig. 1D). When the diameter or the depth was insufficient, array rate was decreased, and when they were too great, fluorescence signals of two to three cells were observed under a fluorescence microscope (data not shown). In this study, well size and shape were optimized to those of lymphocytes, so that we observed single fluorescence signals from each well, as shown in Figure 1C.

Recently, Deutsch et al. reported a live cell array to perform cell-based assays on thousands of individual cells (7).

Microcavities were arrayed in a honeycomb-like structure and could monitor cell responses, such as reactive oxygen species generation, on a single-cell basis (23). Biran and Walt reported an optical imaging fiber-based single live cell array for analyzing yeast or bacterial cells (8). These cell arrays were specifically designed for analyzing cells, and it may be difficult to retrieve objective cells from wells without disturbing the surrounding cells. In our cell microarray, each well was separated so that we could retrieve single objective cells without disturbing the surrounding cells.

Therapeutic MoAb have been developed into beneficial and profitable medical products in molecule-targeted therapeutics (24). To produce fully human MoAb, the bacteriophage display method and the Epstein-Barr virus method have been developed (25,26). The bacteriophage display method requires the preparation of a large-scale bacteriophage library ($\sim 10^{11}$ clones) to get an antigen-specific antibody, making the method difficult to perform in ordinary laboratories. With the availability of a cell scanner, microwell array chips, and a micromanipulator, our system is easy to operate and can be performed in any laboratory that is so equipped. Recently, we have developed a prototype of equipment that can automatically perform processes from cell application to cell retrieval, making the system more appropriate as a procedure for producing human MoAb. Concerning the Epstein-Barr virus method, the virus can transform human B-cells to produce human antibodies. Because only a part of the B-cells can be transformed with the virus, the method cannot efficiently screen antigen-specific B-cells. Our system can screen antigen-specific B-cells directly from freshly separated human peripheral blood lymphocytes and produce antigen-specific MoAb.

We showed that the human anti-HBs antibodies that we had produced exhibited neutralization activity to inhibit HBV infection of human hepatocytes. To demonstrate the neutralization activity, we constructed an estimation system using chimeric mice transplanted with human hepatocytes (16). As HBV can infect only fresh human hepatocytes or that of primates, but not that of rodents, examination of neutralization activity has mostly been performed on chimpanzees (27), which is very expensive and might be contrary to the principles of animal welfare. The use of chimeric mice described in this study is simple and not expensive when compared with the conventional method using chimpanzees because mice are small, easy to breed, and much less expensive.

In conclusion, we have demonstrated and described a system for analyzing a large number of cells on a single-cell basis, which can be applied to "cytomics" analysis, and to the production of human MoAb directly from human peripheral blood B-cells. The system might be applicable for analyzing T-cells to detect antigen-specific T-cells and for cloning TCR cDNAs. By changing the chip design, we are able to analyze various kinds of cells such as hybridoma, hepatocytes, and nerve cells as well as lymphocytes. Our technology should expand the horizons of cell analysis as well as the generation of human MoAb for antibody-based therapeutics and diagnosis of hepatitis virus infection.

Acknowledgments

We thank M. Suzuki, I. Maruyama, H. Nakazato, and Y. Shimizu for their helpful contributions to our discussions, T. Nakashima for providing anti-HBs MoAb, S. Hirota for technical assistance, and K. Hata for secretarial assistance.

Literature Cited

1. Valet G, Leary JF, Tarnok A. Cytomics—New technologies: Towards a human cytome project. Cytometry Part A 2004;59A:167–171.
2. Brehm-Stecher BF, Johnson EA. Single-cell microbiology: Tools, technologies, and applications. Microbiol Mol Biol Rev 2004;68:538–559.
3. Abbas AK, Lichtman AH. Cellular and Molecular Immunology. Philadelphia, PA: Saunders; 2003.
4. Ueki Y, Goldfarb IS, Harindranath N, Gore M, Koprowski H, Notkins AL, Casali P. Clonal analysis of a human antibody response. Quantitation of precursors of antibody-producing cells and generation and characterization of monoclonal IgM, IgG, and IgA to rabies virus. J Exp Med 1990;171:19–34.
5. Shokrgozar MA, Shokri F. Enumeration of hepatitis B surface antigen-specific B lymphocytes in responder and non-responder normal individuals vaccinated with recombinant hepatitis B surface antigen. Immunology 2001;104:75–79.
6. Yamamura S, Kishi H, Tokimitsu Y, Kondo S, Honda R, Rao SR, Omori M, Tamiya E, Muraguchi A. Single-cell microarray for analyzing cellular response. Anal Chem 2005;77:8050–8056.
7. Deutsch M, Deutsch A, Shirihai O, Hurevich I, Afrimzon E, Shafran Y, Zurgil N. A novel miniature cell retainer for correlative high-content analysis of individual untethered non-adherent cells. Lab Chip 2006;6:995–1000.
8. Biran I, Walt DR. Optical imaging fiber-based single live cell arrays: A high-density cell assay platform. Anal Chem 2002;74:3046–3054.
9. Szmuness W, Stevens CE, Oleszko WR, Goodman A. Passive-active immunisation against hepatitis B: Immunogenicity studies in adult Americans. Lancet 1981;1(8220, Part 1):575–577.
10. Madou MJ. Fundamentals of Microfabrication: The Science of Miniaturization. Boca Raton, FL: CRC; 2002.
11. Atalla MM. Semiconductor surfaces and films; the Si-SiO_2 system. In: Gatos HC, editor. Properties of Elemental and Compound Semiconductors, Vol. 5. New York: Interscience; 1960. pp 163–181.
12. Laermer F, Schilp A. Method of anisotopically etching silicon patent. U.S. Patent 5,501,893; 1996.
13. Coburn JW, Winters HF. Plasma etching—A discussion of mechanisms. J Vac Sci Technol 1979;16:391.
14. Goodnow CC, Crosbie J, Adelstein S, Lavoie TB, Smith-Gill SJ, Brink RA, Pritchard-Briscoe H, Wotherspoon JS, Loblay RH, Raphael K, Trent RJ, Basten A. Altered immunoglobulin expression and functional silencing of self-reactive B lymphocytes in transgenic mice. Nature 1988;334:676–682.
15. Tateno C, Yoshizane Y, Saito N, Kataoka M, Utoh R, Yamasaki C, Tachibana A, Soeno Y, Asahina K, Hino H, Asahara T, Yokoi T, Furukawa T, Yoshizato K. Near completely humanized liver in mice shows human-type metabolic responses to drugs. Am J Pathol 2004;165:901–912.
16. Tsuge M, Hiraga N, Takaishi H, Noguchi C, Oga H, Imamura M, Takahashi S, Iwao E, Fujimoto Y, Ochi H, Chayama K, Tateno C, Yoshizato K. Infection of human hepatocyte chimeric mouse with genetically engineered hepatitis B virus. Hepatology 2005;42:1046–1054.
17. Mercer DF, Schiller DE, Elliott JF, Douglas DN, Hao C, Rinfret A, Addison WR, Fischer KP, Churchill TA, Lakey JR, Tyrrell DL, Kneteman NM. Hepatitis C virus replication in mice with chimeric human livers. Nat Med 2001;7:927–933.
18. Cooke MP, Heath AW, Shokat KM, Zeng Y, Finkelman FD, Linsley PS, Howard M, Goodnow CC. Immunoglobulin signal transduction guides the specificity of B cell-T cell interactions and is blocked in tolerant self-reactive B cells. J Exp Med 1994;179:425–438.
19. Gee KR, Brown KA, Chen WN, Bishop-Stewart J, Gray D, Johnson I. Chemical and physiological characterization of fluo-4 Ca(2+)-indicator dyes. Cell Calcium 2000;27:97–106.
20. Bancroft WH, Mundon FK, Russell PK. Detection of additional antigenic determinants of hepatitis B antigen. J Immunol 1972;109:842–848.
21. Bonn D. Biocomplexity: Look at the whole, not the parts. Lancet 2001;357:288.
22. Freeman WJ, Kozma R, Werbos PJ. Biocomplexity: Adaptive behavior in complex stochastic dynamical systems. Biosystems 2001;59:109–123.
23. Zurgil N, Shafran Y, Afrimzon E, Fixler D, Shainberg A, Deutsch M. Concomitant real-time monitoring of intracellular reactive oxygen species and mitochondrial membrane potential in individual living promonocytic cells. J Immunol Methods 2006;316:27–41.
24. Reichert JM, Rosensweig CJ, Faden LB, Dewitz MC. Monoclonal antibody successes in the clinic. Nat Biotechnol 2005;23:1073–1078.
25. Rosen A, Persson K, Klein G. Human monoclonal antibodies to a genus-specific chlamydial antigen, produced by EBV-transformed B cells. J Immunol 1983;130:2899–2902.
26. Smith GP. Filamentous fusion phage: Novel expression vectors that display cloned antigens on the virion surface. Science 1985;228:1315–1317.
27. Sawada H, Iwasa S, Nishimura O, Kitano K. Efficient production of anti-(hepatitis B virus) antibodies and their neutralizing activity in chimpanzees. Appl Microbiol Biotechnol 1995;43:445–451.